Tumor-educated Tregs drive organ-specific metastasis in breast cancer by impairing NK cells in the lymph node niche

Kos, K.; Aslam, M.A.; Ven, R. van de; Wellenstein, M.D.; Pieters, W.; Weverwijk, A. van; ... ; Visser, K.E. de

Cell Reports

CellPress
OPEN ACCESS

Article

Tumor-educated T_{regs} drive organ-specific metastasis in breast cancer by impairing NK cells in the lymph node niche

Kevin Kos,[1,2] Muhammad A. Aslam,[1,3,11] Rieneke van de Ven,[4,9,11] Max D. Wellenstein,[1,2,10] Wietske Pieters,[1] Antoinette van Weverwijk,[1,2] Danique E.M. Duits,[1,2] Kim van Pul,[4] Cheei-Sing Hau,[1,2] Kim Vrijland,[1,2] Daphne Kaldenbach,[1,2] Elisabeth A.M. Raeven,[1,2] Sergio A. Quezada,[5] Rudi Beyaert,[6,7] Heinz Jacobs,[1] Tanja D. de Gruijl,[4] and Karin E. de Visser[1,2,8,12,*]

[1]Division of Tumor Biology & Immunology, Netherlands Cancer Institute, 1066 CX Amsterdam, the Netherlands
[2]Oncode Institute, Utrecht, the Netherlands
[3]Institute of Molecular Biology and Biotechnology, Bahauddin Zakariya University, Multan 60800, Pakistan
[4]Department of Medical Oncology, Amsterdam UMC, Vrije Universiteit Amsterdam, Cancer Center Amsterdam and Amsterdam Institute for Infection and Immunity, 1081 HV Amsterdam, the Netherlands
[5]Cancer Immunology Unit, University College London Cancer Institute, WC1E 6DD London, UK
[6]Center for Inflammation Research, Unit of Molecular Signal Transduction in Inflammation, VIB, 9052 Ghent, Belgium
[7]Department of Biomedical Molecular Biology, Ghent University, 9052 Ghent, Belgium
[8]Department of Immunology, Leiden University Medical Center, Leiden, the Netherlands
[9]Present address: Department of Otolaryngology/Head-Neck Surgery, Amsterdam UMC, Vrije Universiteit Amsterdam, Cancer Center Amsterdam and Amsterdam Institute for Infection and Immunity; 1081 HV Amsterdam, the Netherlands
[10]Present address: Hubrecht Institute, Royal Netherlands Academy of Arts and Sciences (KNAW) and University Medical Center Utrecht; 3584 CT Utrecht, the Netherlands
[11]These authors contributed equally
[12]Lead contact
*Correspondence: k.d.visser@nki.nl
https://doi.org/10.1016/j.celrep.2022.110447

SUMMARY

Breast cancer is accompanied by systemic immunosuppression, which facilitates metastasis formation, but how this shapes organotropism of metastasis is poorly understood. Here, we investigate the impact of mammary tumorigenesis on regulatory T cells (T_{regs}) in distant organs and how this affects multi-organ metastatic disease. Using a preclinical mouse mammary tumor model that recapitulates human metastatic breast cancer, we observe systemic accumulation of activated, highly immunosuppressive T_{regs} during primary tumor growth. Tumor-educated T_{regs} show tissue-specific transcriptional rewiring in response to mammary tumorigenesis. This has functional consequences for organotropism of metastasis, as T_{reg} depletion reduces metastasis to tumor-draining lymph nodes, but not to lungs. Mechanistically, we find that T_{regs} control natural killer (NK) cell activation in lymph nodes, thereby facilitating lymph node metastasis. In line, an increased T_{reg}/NK cell ratio is observed in sentinel lymph nodes of breast cancer patients compared with healthy controls. This study highlights that immune regulation of metastatic disease is highly organ dependent.

INTRODUCTION

The main cause of breast cancer-related mortality is metastatic disease. Over the past decades, breast cancer survival has improved through detection and intervention in early stages of breast cancer, but preventing and treating metastasis remains an unmet clinical need (DeSantis et al., 2019). Disseminated cancer cells progress through a multistep cascade, which involves complex interactions between cancer and host cells, including immune cells (Lambert et al., 2017). The immune system plays a dual role in metastasis formation. While properly activated cytotoxic immune cells are equipped to control metastasis, tumor-induced immunosuppressive immune cells exploit a diversity of mechanisms to promote metastasis (Garner and de Visser, 2020). Emerging data indicate that tissue tropism of metastasis may be influenced by the immune contexture in distant organs, suggesting an additional layer of complexity in metastasis formation (Angelova et al., 2018). However, how immunosuppressive mechanisms differ per metastatic site, and how this shapes tissue tropism of metastasis, is poorly understood.

An important cell type involved in immunosuppression in cancer is the $CD4^+FOXP3^+$ regulatory T cell (T_{reg}) (Kos and de Visser, 2021; Plitas et al., 2016; Plitas and Rudensky, 2020). In breast cancer, immunosuppressive T_{regs} densely populate human tumors, and high levels of intratumoral T_{regs} correlate with high

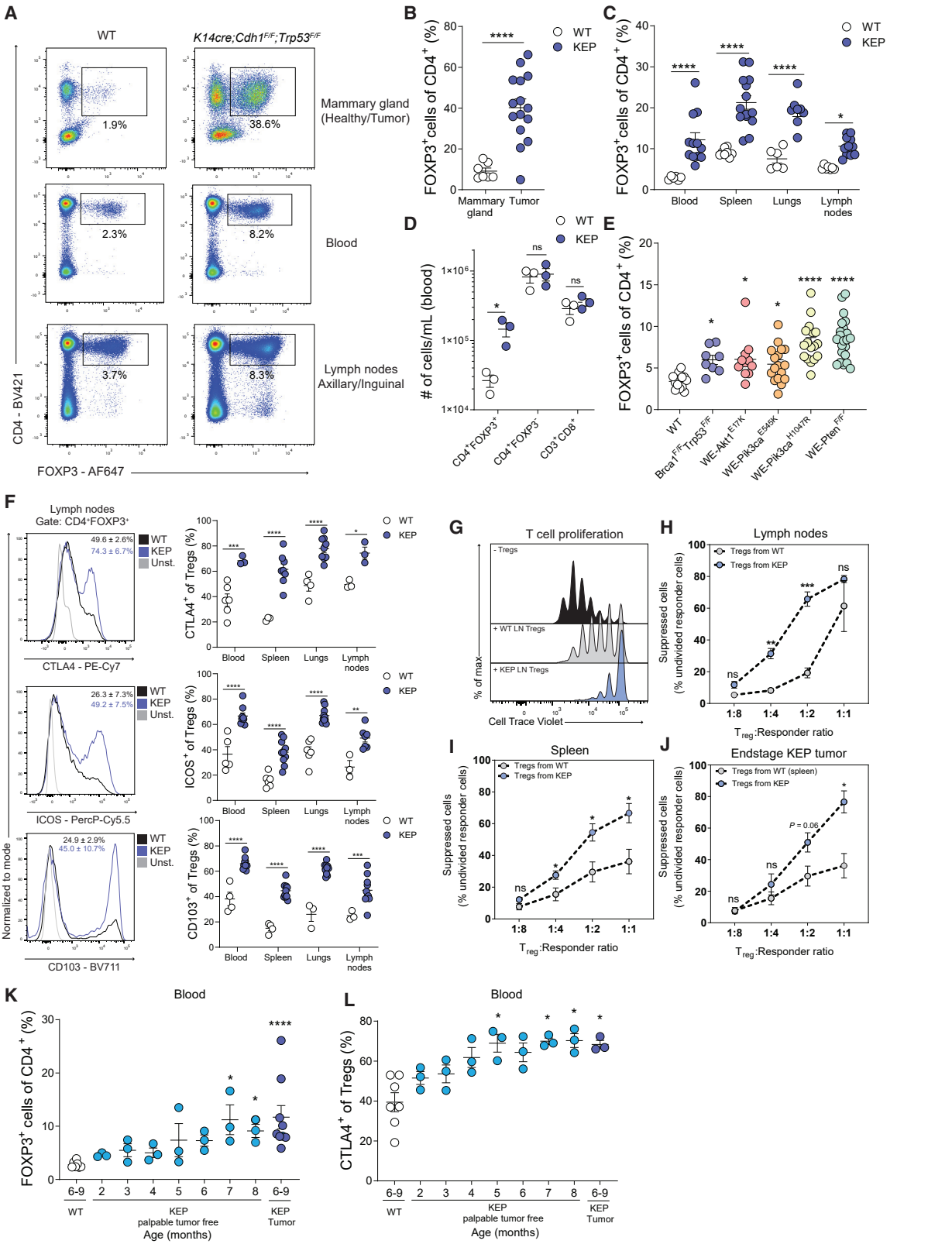

(legend on next page)

tumor grade and poor survival (Liu et al., 2014; Plitas et al., 2016). Intriguingly, clinical data suggest that primary breast tumors affect T_{regs} beyond the tumor microenvironment. T_{regs} in peripheral blood have been reported to be increased in breast cancer patients (Decker et al., 2012; Liyanage et al., 2002; Perez et al., 2007; Wolf et al., 2003), and their responsiveness to cytokine stimulation is predictive of breast cancer relapse (Wang et al., 2019). In addition, recent studies have shown that T_{regs} accumulate in sentinel lymph nodes (LNs) of breast cancer patients, which correlates with cancer spread to these LNs (Faghih et al., 2014; Jiang et al., 2015; Mansfield et al., 2009; Núñez et al., 2020; van Pul et al., 2019), suggesting a potential role for T_{regs} in modulating metastasis to tumor-draining LNs.

Despite these intriguing clinical observations, and the attention that tumor-associated T_{regs} have received in the context of breast cancer in recent years (Clark et al., 2020; Kos and de Visser, 2021), the lack of preclinical models that closely recapitulate human multi-organ metastatic disease has limited our understanding of the importance of T_{regs} in cancer spread to different distant organs (Gómez-Cuadrado et al., 2017). Preclinical studies performed with mouse models based on orthotopic inoculation of breast cancer cell lines have shown that ablation of T_{regs} can attenuate primary tumor growth and subsequent metastasis formation to the lungs (Bos et al., 2013; Hughes et al., 2020; Liu et al., 2016). However, research on T_{regs} in the context of cancer is mostly focused on their role in the microenvironment of primary tumors or metastases. The systemic impact of primary tumors on T_{regs} in distant organs, and their functional significance for metastasis formation in different tissue contexts, has remained largely unclear. Additionally, the role of T_{regs} in hallmarks of metastatic disease such as systemic immunosuppression and the development of a pre-metastatic niche is understudied (Garner and de Visser, 2020), and therefore remains elusive.

Here we describe how mammary tumors systemically rewire T_{regs}, and how this affects metastatic disease to different organs. To achieve this, we utilized models that allow for interrogation of tissue-specific metastasis, i.e. the transgenic *K14cre;Cdh1$^{F/F}$;Trp53$^{F/F}$* (KEP) mouse model of invasive mammary tumorigenesis (Derksen et al., 2006), and the KEP-based mastectomy model for spontaneous multi-organ metastatic disease (Doornebal et al., 2013). We observed systemic accumulation of activated, highly immunosuppressive T_{regs} during primary tumor growth. These T_{regs} showed striking tissue-specific transcriptional rewiring in response to mammary tumorigenesis, and elicited a tissue-specific effect on metastasis formation, as neo-adjuvant depletion of T_{regs} reduced cancer spread to axillary (Ax) LNs, but not to the lungs. Mechanistically, we demonstrate that T_{regs} promote LN metastasis formation through inhibition of NK cells in the LN niche. These findings add another mechanism to the emerging body of literature that immune regulation of metastatic disease is highly organ dependent, warranting a more personalized approach in the fight against metastatic disease.

RESULTS

Primary mammary tumors induce systemic expansion and activation of T_{regs}

To assess whether *de novo* mammary tumor formation exerts a systemic impact on T_{regs}, we examined the abundance, phenotype, and activation status of T_{regs} in tumors, blood, and distant organs of the KEP mouse model, which spontaneously develops mammary tumors at 6–8 months of age resembling human invasive lobular carcinomas (ILCs) (Derksen et al., 2006). We observed that mammary KEP tumors are highly infiltrated by FOXP3$^+$CD4$^+$ T cells, compared with healthy mammary glands of age-matched wild-type (WT) littermate controls (Figures 1A and 1B). Interestingly, increased frequencies and absolute counts of T_{regs} were also observed in blood and in loco-regional or distant organs that are conducive to metastatic spread such as tumor-draining LNs (TDLNs; axillary and inguinal, dependent on the location of the primary mammary tumor), spleen, lungs, and non-draining LNs (NDLNs) of KEP mice bearing end-stage mammary tumors (225 mm^2) (Figures 1A, 1C, S1A, and S1B). Notably, we did not find a relative increase in CD4$^+$FOXP3$^-$, or CD8$^+$ T cells (with the exception of CD8$^+$ T cells in TDLNs) in tumor-bearing KEP mice (Figures 1D, S1C, and S1D). An increase in absolute cell counts was also observed for CD4$^+$FOXP3$^-$ and

Figure 1. Primary mammary tumors induce systemic expansion and activation of CD4$^+$FOXP3$^+$ T cells

(A) Representative dot plots depicting the CD4$^+$FOXP3$^+$ T_{reg} population (%) gated on live, CD45$^+$CD3$^+$ cells in indicated tissues of *K14cre;Cdh1$^{F/F}$;Trp53$^{F/F}$* (KEP) mice bearing mammary tumors (225 mm^2) versus WT controls.

(B and C) Frequencies of FOXP3$^+$ cells of CD4$^+$ T cells in indicated tissues of KEP mice bearing mammary tumors (225 mm^2) versus WT controls (n = 6–15 mice/group) as determined by flow cytometry.

(D) Quantification of absolute cell counts of indicated adaptive immune cell populations per milliliter of blood of KEP mice bearing mammary tumors (225 mm^2) versus WT controls (n = 3 mice/group).

(E) Frequencies of FOXP3$^+$ cells of CD4$^+$ T cells in blood of mice bearing end-stage tumors of indicated transgenic mouse models for mammary tumorigenesis compared with age-matched WT mice (n = 8–22 mice/group).

(F) Representative histograms depicting expression (left) and quantification (right) of CTLA4, ICOS, and CD103 gated on CD4$^+$ FOXP3$^+$ T cells, in indicated tissues of KEP mice (blue) bearing tumors (225 mm^2) versus WT littermates (black) by flow cytometry (n = 3–11 mice/group).

(G) Representative histogram plots of Cell Trace Violet (CTV) expression in activated CD4/CD8 T cells alone (black) or upon co-culture with CD4$^+$CD25$^+$ cells (gray and blue) obtained from indicated tissues at 1:2 T_{reg}:responder ratio.

(H–J) Quantification of undivided responder cells (CD8$^+$ and CD4$^+$ T cells) based on CTV expression, upon co-culture with CD4$^+$CD25$^+$ isolated from indicated tissues at various ratios (data pooled from three to four independent experiments, with two technical replicates per experiment).

(K) Frequencies of FOXP3$^+$ cells of CD4$^+$ T cells in blood of tumor-free, tumor-bearing (225 mm^2) KEP mice and WT controls (n = 3–9 mice/group).

(L) Frequencies of CTLA4$^+$ cells of FOXP3$^+$CD4$^+$ T cells in blood of tumor-free, tumor-bearing (225 mm^2) KEP mice and WT controls (n = 3–7 mice/group). Data in (B)–(F), (H)–(L) show mean ± SEM p values determined by unpaired Student's t test (B, D, H, I, J), one-way ANOVA with Dunnett's multiple comparison test (E), two-way ANOVA with Sidak's multiple comparison test (C and F), and Kruskal-Wallis test with Dunn's multiple comparison test (K and L). Asterisks indicate statistically significant differences compared with WT. *p < 0.05, **p < 0.01, ***p < 0.001, ****p < 0.0001.

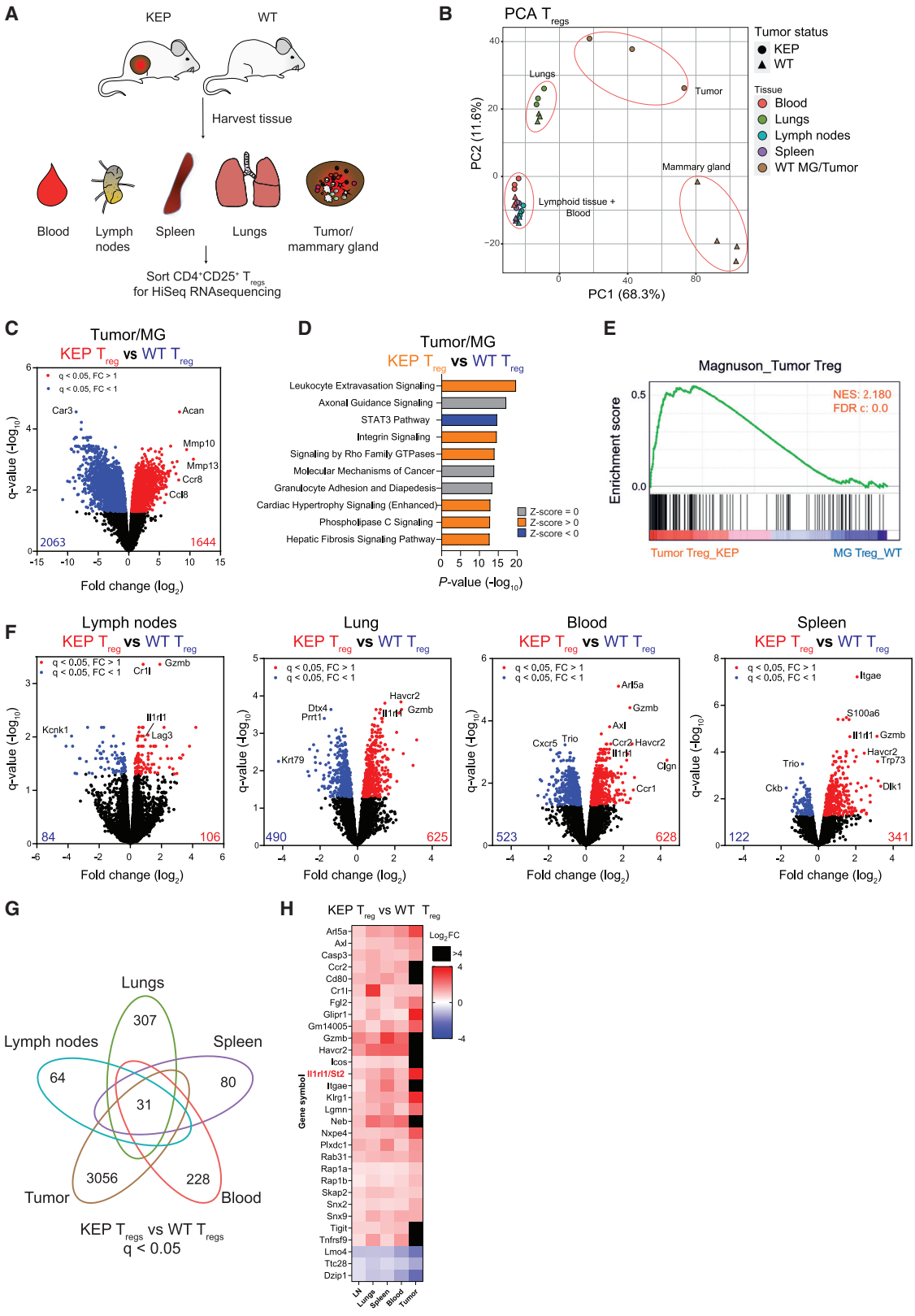

(legend on next page)

$CD8^+$ T cells in LNs and tumors (Figures S1E–S1G), due to expansion of these tissue compartments in KEP mice versus WT controls. However, comparing the ratio of $FOXP3^+/CD8^+$ and $FOXP3^+/FOXP3^-$ cells in different tissues of tumor-bearing KEP mice and WT controls (Figures S1H and S1I) confirmed that mammary tumorigenesis specifically and systemically expands T_{regs} among the adaptive immune cell compartment.

We then assessed whether T_{reg} expansion is explained by their increased proliferation or survival in tumor-bearing KEP mice. Ki67 expression on T_{regs} in tumor-bearing KEP mice was found to be uniquely increased in LNs, compared with WT controls (Figure S1J). Notably, no difference was observed between TDLNs and NDLNs, showing T_{reg} proliferation is systemically increased in LNs of tumor-bearing KEP mice (Figure S1K). Furthermore, KEP T_{regs} showed increased viability when exposed to serum obtained from tumor-bearing KEP mice, as opposed to serum obtained from WT mice (Figure S1L). Combined, these data suggest that LNs may be an important site for T_{reg} proliferation in KEP mice, and that a soluble factor in KEP serum may contribute to increased T_{reg} survival.

To investigate whether this systemic increase of T_{regs} is consistently observed across preclinical mouse models of breast cancer, we analyzed T_{reg} frequency in five different transgenic mouse models that represent different subsets of human breast cancers (Figure 1E). Indeed, we found T_{regs} to be significantly increased in the blood of tumor-bearing mice of all five models compared with WT controls, indicating systemic T_{reg} expansion is a prevalent feature of mammary tumorigenesis.

Using high-dimensional flow cytometry, we observed that T_{regs} both in- and outside of mammary tumors have increased expression of surface proteins associated with T_{reg} activation and suppressor function including cytotoxic T lymphocyte-associated protein 4 (CTLA4), inducible T cell co-stimulator (ICOS), and CD103 in KEP tumor-bearing mice compared with WT controls, showing that these cells undergo a profound phenotypic change during mammary tumor progression (Figures 1F, S1M, and S1N). To address whether the enhanced activation state of KEP T_{regs} affects their functionality throughout the tumor-bearing host, we used fluorescence-activated cell sorting (FACS) to sort T_{regs} from TDLNs, spleen, and tumors from KEP mice and WT controls to assess their suppressive activity on the proliferation of $CD4^+$ and $CD8^+$ T cells *in vitro*. Regardless of the tissue of origin, T_{regs} from tumor-bearing mice were significantly more potent in suppressing T cell proliferation compared with T_{regs} isolated from WT mice (Figures 1G–1J), indicating that tumor-educated T_{regs} have enhanced immunosuppressive potential, both intratumorally as well as in TDLNs and spleen.

We next determined the dynamics of T_{reg} accumulation and education by following T_{reg} frequency and phenotype in aging KEP mice (from 2 to 8 months of age). Around 3 months of age, most KEP mice display microscopic neoplastic lesions in their mammary glands, which, over time, progress into palpable mammary tumors, with a median latency of 6–8 months (Derksen et al., 2006). T_{reg} frequency in blood gradually increased during neoplastic progression in KEP mice, and was significantly increased in KEP mice of 7 months and older prior to the onset of palpable mammary tumors, compared with age-matched controls (Figure 1K). Further analysis of these T_{regs} showed that the impact of mammary tumorigenesis on T_{reg} phenotype showed different kinetics per protein. Although the expression of CTLA4 increased prior to the development of palpable tumors, the expression of ICOS and CD103 was exclusively increased in tumor-bearing KEP mice (Figures 1L, S1O, and S1P). Together, these data demonstrate that primary mammary tumorigenesis engages T_{regs} beyond the tumor microenvironment, leading to their systemic expansion and activation.

Mammary tumors alter the transcriptome of T_{regs} in tumors and distant organs

To delineate the impact of mammary tumor progression on T_{regs} in distant organs, RNA sequencing (RNA-seq) was performed on T_{regs} ($CD4^+CD25^{high}$) isolated from blood, TDLNs, lungs, spleens, healthy mammary glands, and mammary tumors (225 mm^2) from tumor-bearing KEP mice and WT controls (Figure 2A). Importantly, $CD4^+CD25^{high}$ cells isolated from these tissues showed high and equal FOXP3 expression (Figure S2A). Principal component analysis (PCA) showed distinct clustering of T_{regs}, based on their residence in either lymphoid tissue (spleen and LNs) and blood, or residence in peripheral tissue (lungs, tumor, mammary gland) (Figure 2B). Furthermore, T_{regs} residing in distant organs cluster together independent of tumor status, whereas the gene expression profiles of tumor and mammary gland T_{regs} appear very distinct. Indeed, differential gene expression analysis comparing intratumoral KEP T_{regs} and mammary tissue-resident T_{regs} revealed 3,707 differentially expressed genes (Figure 2C). Ingenuity pathway analysis (IPA) showed the significantly changed pathways between T_{regs}

Figure 2. Mammary tumor formation affects T_{reg} gene expression in distant sites

(A) Schematic overview of experiment.

(B) PCA plot of transcriptomic profiles of T_{regs}. Each symbol represents one sample of sequenced T_{regs}.

(C) Volcano plots showing differentially expressed genes ($q < 0.05$) comparing T_{regs} isolated from tumors of KEP mice versus healthy mammary gland of WT controls.

(D) IPA on differentially expressed genes ($q < 0.05$) comparing T_{regs} isolated from tumors of KEP mice versus healthy mammary gland of WT controls. Top 10 statistically significant pathways are shown.

(E) GSEA comparing KEP/WT T_{regs} isolated from tumors and healthy mammary gland with TIT_{reg} gene set (Magnuson et al., 2018). Normalized enrichment score (NES) and false discovery rate (FDR) indicated.

(F) Volcano plots showing differentially expressed genes ($q < 0.05$) from T_{regs} isolated from indicated tissues of tumor-bearing KEP mice versus WT controls. Red indicates upregulated in KEP, blue indicates upregulated in WT.

(G) Venn diagram showing distribution of differentially expressed genes ($q < 0.05$) identified by comparing gene expression of T_{regs} isolated from tumor-bearing KEP mice versus WT controls for each tissue.

(H) Heatmap depicting Log_2FC change of 30 shared KEP T_{reg} genes up-/downregulated in KEP T_{regs} across tissue ($q < 0.05$, KEP T_{reg} versus WT T_{reg} per tissue).

from tumors and mammary glands to pertain to cell migration and extravasation (Figure 2D), which is underscored by some of the most differentially expressed genes, including *Mmp10*, *Mmp13*, and *Ccr8* (Table S1). We confirmed by gene set enrichment analysis (GSEA) that intratumoral KEP T_{regs} are significantly enriched for a clinically relevant cross-species and cross-tumor model tumor-infiltrating T_{regs} (TIT_{regs}) signature (Magnuson et al., 2018) (Figure 2E).

Next, we sought to explore how mammary tumorigenesis affects T_{regs} in distant organs by comparing gene expression profiles of KEP versus WT T_{regs} from matched tissues. This comparison identified differential gene regulation in T_{regs} in all organs tested, indicating that mammary tumors induce systemic transcriptional changes in T_{regs} (Figure 2F). To further map these differentially regulated genes and their occurrence across different tissues, we analyzed their distribution in KEP versus WT T_{regs} across tissues (Figure 2G). Doing so, we identified a set of 31 core genes to be significantly different (27 upregulated, three downregulated, one bidirectional, dependent on tissue) in KEP T_{regs} regardless of tissue residence, suggesting a certain level of convergent, tissue-independent transcriptional rewiring in response to mammary tumorigenesis (Figure 2H). Among those upregulated, we found genes encoding proteins important for T cell activation and the immunosuppressive features of T_{regs}, such as *Icos*, *Klrg1*, *Havcr2*, *Tigit*, and *Tnfrsf9*. KEP T_{regs} were also found to have enhanced gene expression of *Gzmb*, which is known for its cytolytic function in NK and $CD8^+$ T cells, but has been shown to contribute to immunosuppression when expressed by T_{regs} (Cao et al., 2007). Combined, these data suggest that mammary tumorigenesis enhances systemic immunosuppression through transcriptional rewiring of T_{regs} in distant organs.

We additionally identified *Il1rl1*, a gene encoding the IL-33 receptor ST2, to be systemically increased in KEP T_{regs} compared with WT T_{regs}, which was confirmed by FACS analysis (Figures S2B and S2C). Interleukin (IL)-33/ST2 signaling on T_{regs} has recently been described to induce a pro-tumorigenic phenotype in intratumoral T_{regs} (Li et al., 2019; Pastille et al., 2019; Son et al., 2020) and has also been shown to drive expansion of T_{regs} *in vitro* and *in vivo* (Matta and Turnquist, 2016). In KEP mice, IL-33 was found to be significantly increased in TDLNs compared with WT LNs, which was not observed in blood, tumor, or lungs (Figure S2D). Nevertheless, short-term neutralization of IL-33 in tumor-bearing KEP mice utilizing two independent approaches, i.e., treatment of mice with anti-IL-33 or with an IL-33 antagonist (IL-33 Trap, Holgado et al., 2019) (Figure S2E), did not alter systemic T_{reg} accumulation, proliferation, or phenotype (Figures S2F–S2I), suggesting that, in mice with established mammary tumors, the presence of the $ST2^+$ T_{reg} population is maintained independent of endogenous IL-33.

Taken together, these data demonstrate that mammary tumorigenesis induces systemic transcriptional rewiring of T_{regs}, sharing a core set of genes associated with T_{reg} function and activation.

The impact of mammary tumorigenesis on T_{regs} is dictated by the tissue context

In addition to transcriptional commonalities observed in KEP T_{regs} in distant organs, we identified a large number of tumor-induced genes in KEP T_{regs} that were not shared across multiple tissues, but rather were dependent on the tissue context (Figure 2G), indicating that the local environment shapes the response of T_{regs} to mammary tumorigenesis. Therefore, we continued our characterization of T_{regs} in distant organs of tumor-bearing KEP mice by exploring the impact of the tissue context. To do so, we omitted tumors and mammary glands from the dataset and re-analyzed the T_{reg} transcriptome. PCA analysis revealed that T_{regs} derived from the same tissues cluster together, indicating that tissue residence is a more dominant factor for the transcriptional state of T_{regs} than the presence or absence of a primary mammary tumor (Figure 3A). To elaborate the relationship between T_{regs} in different tissues, we performed correlation analysis, and found T_{regs} from LNs, spleen, and blood to be relatively closely correlated, whereas lung T_{regs} were very distinct (Figure 3B). Interestingly, visualization of differentially regulated genes of matched tissues in a force-directed graph (KEP versus WT T_{regs}, $q < 0.05$) (Sun et al., 2019a) revealed complex relationships between clusters of genes dependent on the tissue context (Figure 3C). Among these, roughly 30% of differentially regulated genes in KEP T_{regs} versus WT T_{regs} were found to be tissue specific (74 out of 183 genes in LN, 379 out of 1,100 genes in lung, 417 out of 1,129 genes in blood, 107 out of 462 genes in spleen), indicating that KEP T_{regs} in distant organs acquire a unique tissue-specific transcriptional profile (Figure 3C, Table S1). We next performed IPA to interrogate which molecular pathways are associated with the differentially expressed genes between KEP and WT T_{regs} in distant organs. Notably, we identified several pathways related to T cell effector states (T-helper 1 [Th1] pathway, T-helper 2 [Th2] pathway, T helper cell differentiation, Th1 and Th2 activation pathway) to be shared among KEP T_{regs} in multiple distant organs (Figure 3D). In addition to shared pathways, we also found several pathways that were only observed for specific tissues, such as integrin signaling in blood T_{regs} and apoptosis signaling in lung T_{regs}, highlighting the differential impact of mammary tumorigenesis on T_{regs} in distant organs.

Taken together, these data demonstrate that the mammary tumor-induced changes in T_{regs} are strongly influenced by their tissue context, raising the question of whether these site-specific differences may have functional consequences for the progression of breast cancer.

Tumor-educated T_{regs} promote LN metastasis but not lung metastasis

As we observed systemic and organ-specific mammary tumor-induced alterations of T_{regs}, we set out to explore the impact of T_{regs} on multi-organ metastatic disease utilizing the KEP-based mastectomy model of spontaneous breast cancer metastasis (Figure 4A) (Coffelt et al., 2015; Doornebal et al., 2013). In this model, after orthotopic transplantation of a KEP-derived tumor fragment followed by surgical removal of the outgrown tumor, mice develop overt multi-organ metastatic disease, mainly in Ax TDLNs and lungs. Like primary tumor formation, metastatic disease is also accompanied by the accumulation of T_{regs}, with elevated expression of ICOS, CTLA4, and ST2, compared with non-transplanted naive controls (Figures S3A–S3E).

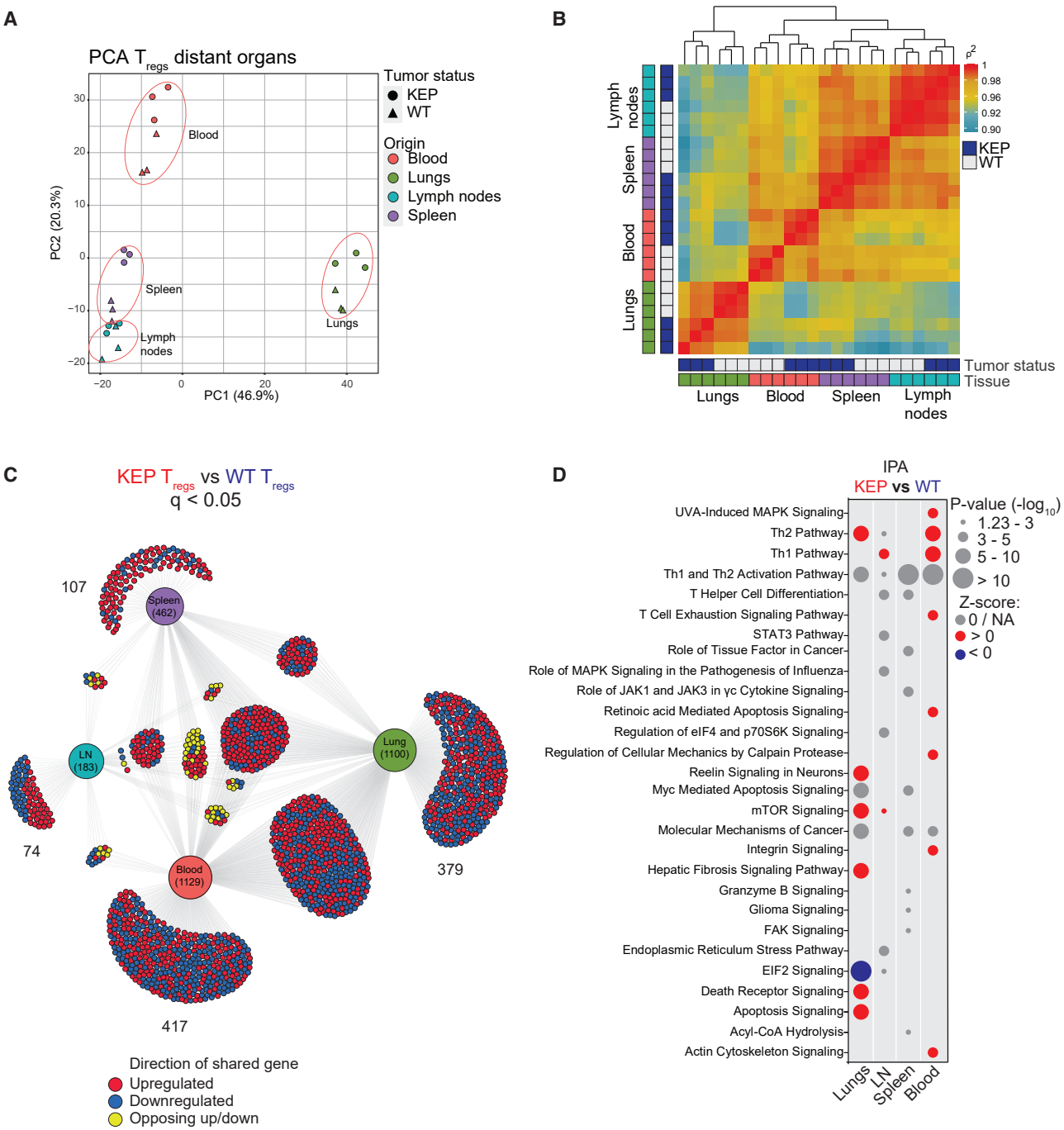

Figure 3. Tissue-dependent transcriptional changes in KEP T_{regs}

(A) PCA plot of transcriptional profiles of T_{regs} isolated from distant organs and blood of KEP mice bearing end-stage tumors and WT controls.

(B) Correlation plot matrix plot showing Spearman coefficient between transcriptional profiles of T_{regs} isolated from distant organs and blood of KEP mice bearing end-stage tumors and WT controls.

(C) Force-directed graph depicting differentially expressed genes between KEP T_{regs} and WT T_{regs} ($q < 0.05$). Genes identified by comparing gene expression of T_{regs} isolated from distant organs and blood of tumor-bearing KEP mice versus WT controls for each tissue, depicted by DiVenn (Sun et al., 2019a).

(D) IPA on differentially expressed genes ($q < 0.05$) comparing T_{regs} isolated from indicated tissues of KEP mice bearing end-stage tumors versus WT controls. Top 10 significant pathways are shown for each tissue.

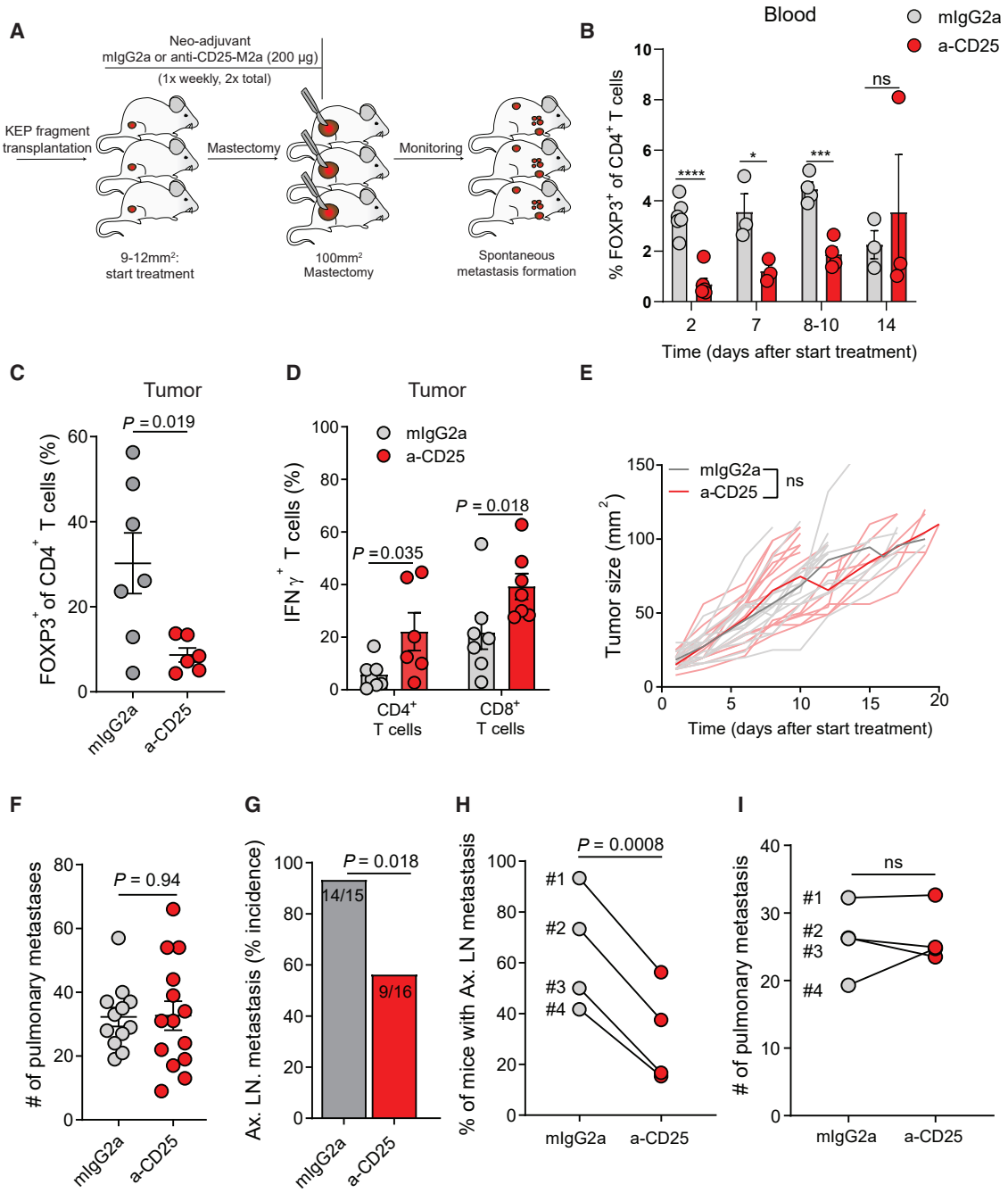

Figure 4. Tumor-educated T_{regs} promote LN metastasis but not lung metastasis

(A) Schematic overview of study (n = 15–16 mice/group).

(B) Frequency of FOXP3$^+$ cells of CD4$^+$ T cells in mice bearing transplanted KEP tumors, treated with mIgG2a or anti-CD25 at indicated timepoints after start of treatment (n = 3–6 mice/group).

(C) Intratumoral frequency of FOXP3$^+$ cells in mastectomized tumors, gated on live, CD45$^+$, CD3$^+$, CD4$^+$ T cells as determined by flow cytometry (n = 6–7 mice/group).

(D) Frequency of IFNγ$^+$ cells of CD4$^+$ and CD8$^+$ T cells, in 100-mm^2 mastectomized KEP tumors of mice treated with neo-adjuvant mIgG2a and anti-CD25 as determined by flow cytometry (n = 6–7 mice/group) following a 3-h *ex vivo* stimulation.

(E) Primary tumor growth kinetics of mice bearing transplanted KEP tumors, treated with mIgG2a or anti-CD25.

(F) Number of pulmonary metastases in mice treated with neo-adjuvant mIgG2a and anti-CD25 (n = 12–14 mice/group).

(G) Percentage and number of mice with detectable micro-/macroscopic metastases in Ax TDLNs, in mice treated with neo-adjuvant mIgG2a and anti-CD25 (n = 15–16 mice/group).

(legend continued on next page)

To assess the functional significance of T_{regs} during early metastasis formation, we treated mice in the neo-adjuvant setting with a recently developed Fc-modified antibody, targeting the IL2Rα receptor, CD25 (anti-CD25-M2a), which has been described to efficiently and specifically deplete T_{regs} in tumors and peripheral tissue (Arce Vargas et al., 2017). Indeed, anti-CD25-M2a treatment efficiently depleted $FOXP3^+CD4^+$ T cells from tumors, spleen, LNs, lungs, and circulation in mice bearing transplanted KEP tumors (Figures 4B and 4C, S3F, and S3G). Depletion of T_{regs} was observed for up to 10 days after start of treatment in blood. Although anti-CD25-M2a treatment resulted in increased interferon gamma (IFNγ) expression in both intratumoral $CD4^+$ and $CD8^+$ T cells (Figure 4D), consistent with the concept that tumor-induced T_{regs} are immunosuppressive, we did not observe an effect on primary tumor growth (Figure 4E). Similarly, depletion of T_{regs} in mammary tumor-bearing transgenic KEP mice did not affect primary tumor growth or survival (Figure S3H).

After mastectomy, mice were monitored for the development of overt metastases. While neo-adjuvant T_{reg} depletion did not improve metastasis-related survival or reduce the number of lung metastases (Figures 4F and S3I), micro- and macroscopic analysis of Ax TDLNs (Figure S3J) revealed that anti-CD25-M2a-treated mice developed significantly fewer LN metastases compared with controls (Figure 4G). The incidence of LN metastasis of control mice was 93% (14 out of 15), which was reduced to 56% (9 out of 16) upon anti-CD25-M2a treatment. No difference was observed in the size of LN metastases that did develop in both groups (Figure S3K). The observation that T_{reg} depletion reduces the incidence of LN metastasis by ~50%, but does not affect lung metastasis, was consistent across four independent experimental KEP tumor donors, even though LN metastasis incidence of control groups varied between 41.67% and 93.3% in a donor-dependent fashion (Figures 4H and 4I). These findings indicate that T_{regs} promote metastasis formation, leading to increased incidence of LN metastasis, but also reveals that the impact of T_{regs} on metastasis formation is dependent on the tissue context since lung metastases remain unaffected.

T_{regs} differentially modulate NK cell activation in the LN and lung niche

To gain more insight into how T_{regs} promote metastasis formation in Ax LNs, we first explored the potential role of $CD8^+$ T cells in controlling LN metastasis formation upon T_{reg} depletion, as we found that T_{regs} suppress IFNγ expression by $CD8^+$ T cells in the primary tumor microenvironment (Figure 4D). To do so, we co-depleted $CD8^+$ T cells (Figure S4A) and T_{regs} in the KEP metastasis model, but did not find a difference in LN metastasis incidence between anti-CD25 and anti-CD25/CD8 treatment (Figure 5A), suggesting that the reduced LN metastasis incidence upon depletion of T_{regs} is not linked to intratumoral activation of $CD8^+$ T cells (Figure 4D). Since we observed systemic activation and rewiring of highly immunosuppressive T_{regs} in response to tumorigenesis, we next hypothesized that T_{regs} may differentially facilitate metastasis formation through tissue-specific interactions in the local metastatic niche, independent of their activity in the primary tumor.

To study this as close to the *in vivo* situation as possible, we assessed the impact of tumor-educated T_{regs} on immune cells with potential anti-tumor activity in Ax TDLNs *in vivo*, instead of using traditional *in vitro* suppression assays in which cells may lose their functionality imposed by their respective tissue-microenvironment. *In vitro* suppression assays therefore fail to reproduce the complex interactions that exist *in vivo*, rendering these assays of limited value for studying metastatic niche-dependent processes. Instead, we depleted T_{regs} in mice bearing transplanted KEP tumors and analyzed the phenotype and function of T and NK cells in Ax TDLNs compared with control-treated and naive mice when primary tumors reached a size of 100 mm^2 *ex vivo*. We also analyzed T and NK cells in tumors, blood, and lungs, to gain insights into the tissue-specific impact of tumor-educated T_{regs} on these cells. Interestingly, increased expression of the cytotoxic molecule granzyme B by NK cells ($CD3^-$, $NKp46^+$, $DX5^+$) was observed in the Ax TDLNs of tumor-bearing mice upon T_{reg} depletion (Figures 5B, 5C, and S4B). Increased granzyme B expression was not observed in NK cells in lungs, blood, and tumor upon T_{reg} depletion despite higher baseline expression compared with Ax TDLNs (Figures S4C–S4E), indicating that tumor-activated T_{regs} interfere with granzyme B expression of NK cells specifically in the Ax LN niche. Next, we analyzed the surface expression of CD107a on NK cells as a readout for their degranulation, which is an important mechanism for NK cell cytotoxicity (Paul and Lal, 2017). This showed that NK cells in Ax TDLNs, but not lungs or Ax NDLNs, from T_{reg}-depleted mice cells have increased surface expression of CD107a compared with control treatment (Figures 5D and S4F), showing that Ax TDLN NK cells increase the release of intracellular granules upon T_{reg} depletion *in vivo*. In *in vitro* stimulated NK cells, CD107a expression was not significantly affected by T_{reg} depletion (Figure S4G), suggesting that the impact of T_{regs} on NK cell degranulation is not affecting their intrinsic capacity to degranulate under highly stimulatory conditions, but is rather a result of T_{reg}/NK cell interactions *in vivo*. In contrast, we did not find a significant effect of T_{reg} depletion on T cells in terms of granzyme B, CD107a, IFNγ, tumor necrosis factor alpha (TNFα) expression, or IFNγ by NK cells in Ax TDLNs and lungs (Figures S4H–S4L).

To further dissect the differential impact of T_{regs} on NK cells in the LN and lung niche *in vivo*, we conducted bulk RNA-seq analysis on FACS-sorted NK cells isolated from T_{reg}-depleted and T_{reg}-proficient tumor-bearing mice (Figure 5E). Notably, anti-CD25 induces depletion of T_{regs} via antibody-dependent cell-mediated cytotoxicity (ADCC) through engagement of Fc receptors (Arce Vargas et al., 2017) on innate effector cells,

(H and I) Ax TDLN metastasis incidence (H) and number of lung metastases (I) of each independent experimental donor is shown, in mice receiving weekly neo-adjuvant treatment of 200 μg of mIgG2a or anti-CD25. Symbol indicates an experimental group (mIgG2a/a-CD25), each line connects an independent experimental (donor #1 used in Figures 4G and 4I, n = 15–16 mice/group; donor #2 used in Figure 5A, n = 15–16; donor 3 and 4 used in Figure 6A, n = 30–31 mice/group). Data in (B)–(D) and (F) show mean ± SEM p values determined by unpaired Student's t test (B, C, F), Mann-Whitney test (D), area under curve (AUC) calculation (E), Fisher's exact test (G), and paired Student's t test (H and I).

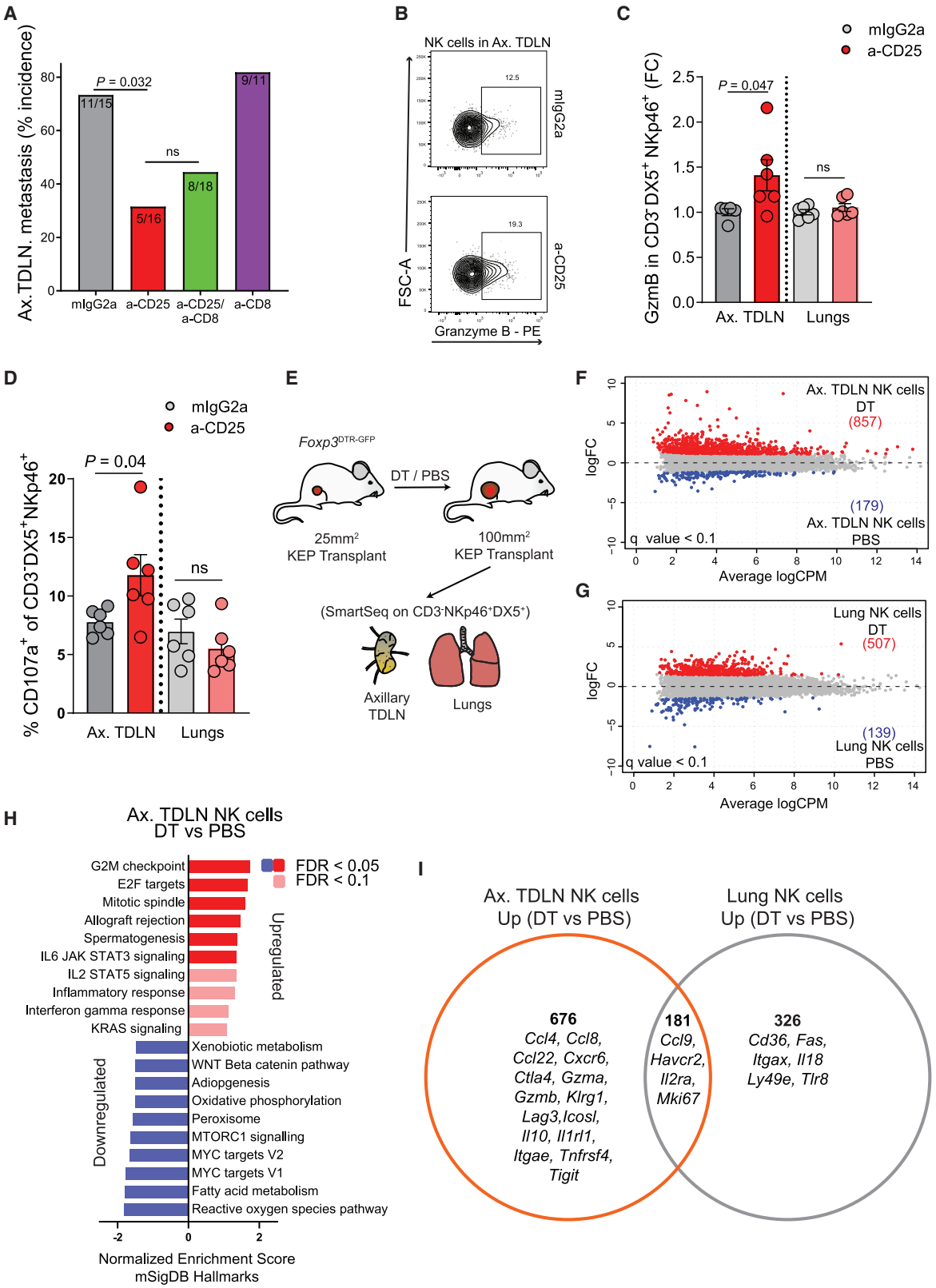

(legend on next page)

including NK cells (Duhan et al., 2019). To confirm that the observed activation of NK cells upon antibody-mediated depletion of T_{regs} is independent of their role in ADCC, we now utilized *Foxp3*$^{DTR-GFP}$ mice in which FOXP3$^+$ cells are efficiently depleted upon injection of diphtheria toxin (DT) (Figure S5A). NK cells were obtained from lungs and Ax TDLNs of PBS or DT-treated *Foxp3*$^{DTR-GFP}$ mice bearing transplanted KEP tumors. Gene expression analysis of NK cells from T_{reg}-depleted versus T_{reg} non-depleted mice identified 1,036 and 646 genes to be differentially expressed in the LNs and lungs respectively, showing that the influence—directly, indirectly, or due to NK cell intrinsic differences—of T_{regs} on the NK cell transcriptome is more pronounced in Ax TDLNs than in lungs (Figures 5F and 5G, Table S2).

To identify which molecular pathways are controlled by T_{regs} in NK cells in tumor-bearing mice, we performed GSEA analysis on the differentially expressed genes of both lung and Ax TDLN NK cells from T_{reg}-depleted versus T_{reg} non-depleted mice using the MSigDB Hallmark Gene sets, which represent 50 well-defined biological processes (Liberzon et al., 2015) (Figures 5H and S5B). We found that the depletion of T_{regs} induces the upregulation of molecular pathways related to DNA replication (G2M checkpoint, E2F targets, mitotic spindle) and inflammation (inflammatory response, IFNγ response) in both Ax TDLN and lung NK cells, suggesting a common role of T_{regs} in curbing NK cell proliferation and activation. However, we also identified pathways that were uniquely upregulated in either Ax TDLN NK cells (IL6-JAK-STAT3 signaling, IL2-STAT5 signaling) or lung NK cells (IFNα response, TNFα signaling via nuclear factor κB [NF-κB]). Although both Ax TDLN and lung NK cells show signs of activation upon depletion of T_{regs} based on GSEA, we identified 676 genes to be uniquely upregulated in Ax TDLN NK cells of T_{reg}-depleted versus T_{reg}-non-depleted mice, compared with 326 in lung NK cells (Figure 5I). Interestingly, a subset of genes found specifically upregulated in Ax TDLN NK cells of T_{reg}-depleted mice encode for proteins with immunomodulatory properties that were not found in lung NK cells of T_{reg}-depleted animals, including *Gzmb*, which we had previously identified in our FACS-based analyses of NK cells (Figures 5B and 5C). Furthermore, we identified other genes encoding for proteins involved in cytotoxicity (*Gzma*, *Serpinb9b*), migration (*Ccl4*, *Ccl8*, *Ccl22*, *Cxcr6*), co-stimulatory receptors (*Icosl*, *Tnfrsf4*), and co-inhibitory receptors (*Tigit*, *Lag3*, *Ctla4*, *Klrg1*), which are indicative of activated NK cells. In summary, these data show that T_{regs} regulate NK cells in a tissue-specific manner, and suggest that tissue context does not only drive T_{reg} phenotype but also affects their interactions with target cells such as NK cells.

T_{regs} promote metastasis through inhibition of NK cells in the LN niche

We next assessed whether the inhibitory effect of T_{regs} on Ax TDLN NK cells affects their capacity to control LN metastasis formation. We performed neo-adjuvant co-depletion of T_{regs} using anti-CD25-M2a and NK cells using anti-NK1.1 in the KEP metastasis model. Anti-NK1.1 efficiently depleted NKp46$^+$DX5$^+$ NK cells in the blood of KEP tumor-bearing mice (Figure S5C). Strikingly, although depletion of T_{regs} significantly reduced the incidence of Ax LN metastasis, combined depletion of T_{regs} and NK cells completely restored LN metastasis formation (Figure 6A). Anti-NK1.1 alone did not alter LN metastasis incidence and none of the treatments affected the number of lung metastases (Figure 6B). Combined, our findings show that tumor-educated T_{regs} repress NK cell activation in Ax TDLNs, thereby curbing their anti-metastatic potential, leading to an increased incidence of LN metastasis. This T_{reg}-mediated immune escape mechanism is specific to the Ax LN, as T_{regs} did not control lung metastasis in this model. Because we did observe some activation of lung NK cells at the transcriptional level in T_{reg}-depleted versus non-depleted mice (Figure 5I), we hypothesized that additional layers of immunosuppression in the lung microenvironment that are independent of T_{regs} may hinder the anti-metastatic potential of lung NK cells. In support of this hypothesis, we found that lung NK cells are mostly terminally differentiated (CD27$^-$CD11b$^+$) in tumor-free mice, but undergo a partial shift toward a non-cytotoxic immature phenotype (CD27$^-$CD11b$^-$) in tumor-bearing mice, independent of T_{regs} (Figure S5D). In contrast to lungs, and in line with previous literature (Chiossone et al., 2009; Hayakawa and Smyth, 2006), Ax TDLN NK cells were found to be mostly in CD27$^+$CD11b$^-$ (immature) and CD27$^+$CD11b$^+$ (cytotoxic) states (Figure S5E), highlighting the differences between NK cells in LNs and lung. Importantly, maturation status in Ax TDLN NK cells was not affected in tumor-bearing mice, suggesting this mechanism is specific to lungs, and potentially contributes to observed differences between lung and LN.

Figure 5. T_{regs} differentially affect NK cells in LN and lungs

(A) Percentage and number of mice with detectable micro-/macroscopic metastases in Ax TDLNs, in mice treated with neo-adjuvant indicated treatments (n = 11–18 mice/group).

(B) Representative dot plot of granzyme B expression by NK cells in Ax TDLNs of mice bearing 100-mm^2 KEP tumors, treated with neo-adjuvant mIgG2a or anti-CD25.

(C) Relative granzyme B expression by NK cells (CD3$^-$DX5$^+$NKp46$^+$) in Ax TDLNs and lungs of mice bearing 100-mm^2 KEP tumors, treated with neo-adjuvant mIgG2a or anti-CD25, following a 3-h *ex vivo* stimulation (n = 6 mice/group). Data are normalized to % GzmB$^+$ of NK cells of control mIgG2a-treated mice.

(D) CD107a expression of NKp46$^+$ DX5$^+$ NK cells from Ax TDLNs and lungs of mice bearing transplanted KEP tumors (100 mm^2) receiving weekly neo-adjuvant treatment of 200 μg of anti-CD25 or mIgG2a (n = 6/group).

(E) Schematic overview of study. Mice received treatment at t = 0 and t = 7 (n = 4 mice/group).

(F and G) MA plot of differentially regulated transcripts for Ax TDLN NK cells (F), and lung NK cells (G) for DT versus PBS treatment. Significantly different transcripts are labeled in red (up), and blue (down).

(H) GSEA analysis of Ax TDLN NK cells, DT versus PBS, using hallmark gene sets. Top 10 enriched up- and downregulated pathways are shown.

(I) Venn diagram depicting distribution of upregulated genes ($q < 0.1$) between Ax TDLN and lung NK cells DT versus PBS treatment. Data in (C) and (D) show mean ± SEM p values determined by Mann-Whitney test (C and D) and Fisher's exact test (A).

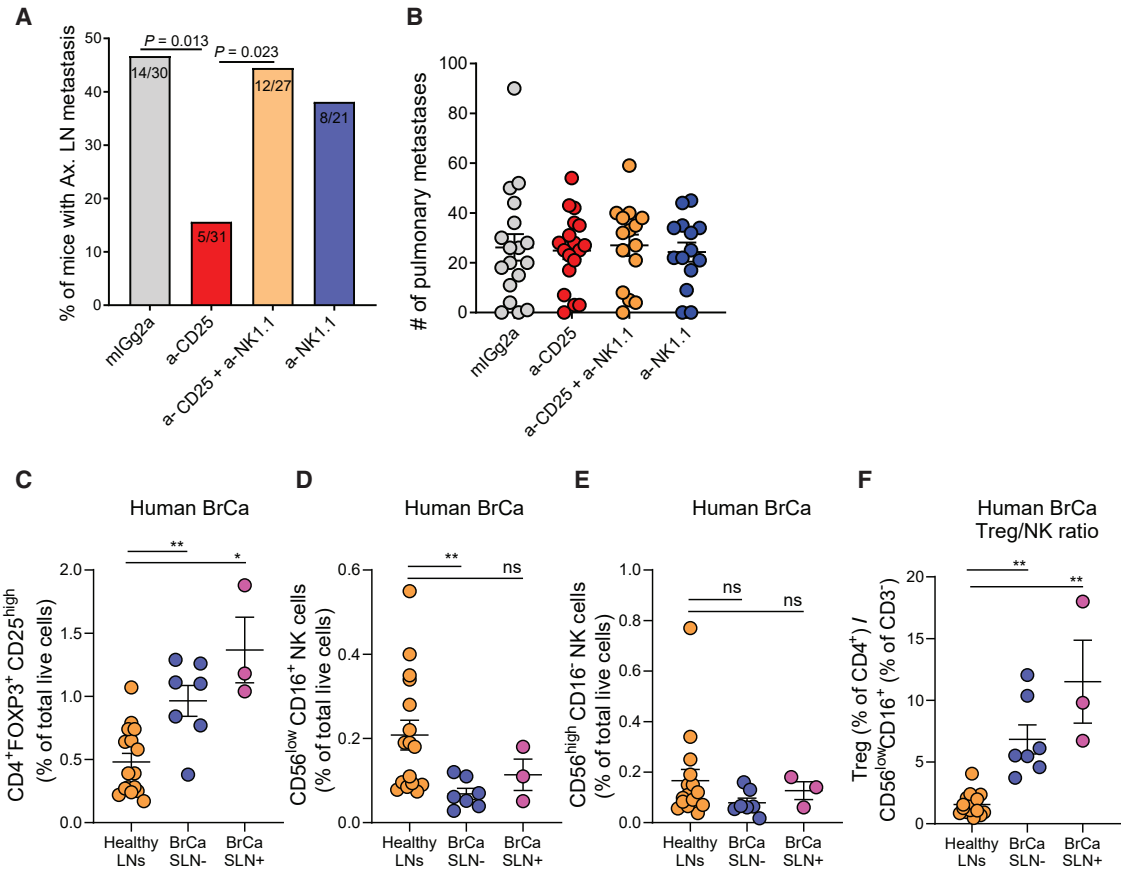

Figure 6. T_{regs} promote axillary LN metastasis through inhibition of NK cells

(A) Percentage and number of mice with detectable micro-/macroscopic metastases in Ax TDLNs, in mice receiving neo-adjuvant treatment as indicated (n = 21–31 mice/group, data pooled from two independent experiments).

(B) Number of pulmonary metastases in mice receiving indicated neo-adjuvant treatment (n = 14–16 mice/group).

(C) Frequencies of $CD3^+CD4^+CD25^+FOXP3^+$ cells of total live cells in human HLNs (n = 16), BrCa tumor-negative (n = 7) and tumor-positive (n = 3) SLNs.

(D and E) Frequencies of indicated subset of NK cells of total live cells in human HLNs (n = 16), BrCa tumor-negative (n = 7) and tumor-positive (n = 3) SLNs.

(F) Ratio of T_{reg} (% of $CD4^+$) versus $CD56^{low}CD16^+$ (% of $CD3^-$) in human HLNs (n = 16), BrCa tumor-negative (n = 7) and tumor-positive (n = 3) SLNs. Data in (B)–(F) show mean ± SEM p values are determined by Kruskal-Wallis test with Dunn's correction for multiple comparisons (C–F), Fisher's exact test (A). $^{**}p < 0.01$, $^{***}p < 0.001$, $^{****}p < 0.0001$.

Reduced NK cells versus increased T_{regs} in sentinel LNs of breast cancer patients

Finally, we validated our preclinical findings on T_{reg} and NK cell interactions in the LN niche of breast cancer patients. To do so, we analyzed the accumulation of T_{regs} ($CD4^+CD25^{high}FOXP3^+$) and NK cells ($CD56^+CD16^-$ and $CD56^{low}CD16^+$) in tumor-free and tumor-positive sentinel LNs of breast cancer patients (BrCa SLN^-/SLN^+), and in Ax LNs from healthy controls (HLNs), using a previously described flow cytometry dataset (van Pul et al., 2019). In line with previous analyses of this unique dataset (van Pul et al., 2019) and consistent with our preclinical data (Figure 1C), T_{reg} levels are significantly elevated in BrCa SLNs compared with HLNs (Figure 6C). We also observed a statistically significant reduction of $CD56^{low}CD16^+$, but not $CD56^+CD16^-$ NK cells, in BrCa SLN^-, and a similar trend in BrCa SLN^+ (Figures 6D and 6E). Notably, in particular $CD56^{low}CD16^+$ have been described to have cytotoxic activity (Poli et al., 2009). Combined, this shifts the T_{reg}/NK cell ratio strongly toward T_{regs} in both tumor-free and tumor-positive BrCa SLNs compared with HLNs (Figure 6F). Despite the low number of BrCa SLN^+ samples, we also observed a non-significant trend of a higher T_{reg}/NK cell ratio in SLN^+ versus SLN^- samples. A rise in T_{regs} in conjunction with a reduction of potentially cytotoxic NK cells in the SLN niche is in accordance with our preclinical finding that LN NK cells have reduced expression of CD107a and the cytotoxic molecule granzyme B under control of T_{regs} in tumor-bearing mice (Figures 5B–5D).

DISCUSSION

Understanding the nature of cancer-associated systemic immunosuppression and its impact on different (pre-)metastatic niches is essential to ultimately design effective therapeutic strategies that prevent or fight metastatic disease. Here, we show that mammary tumorigenesis has an extensive impact on T_{regs}, both intratumorally and in distant organs. Tumor-educated T_{regs}

are highly activated and immunosuppressive, and display tissue-specific adaptation to tumor development. This has functional relevance for metastasis formation, as T_{regs} selectively promote LN metastasis, but not lung metastasis, through inhibition of NK cells. These data highlight the importance of the tissue context for immune escape mechanisms, and reveal a causal role for T_{regs} in the development of LN metastasis.

An extensive number of clinical studies has reported that high infiltration of FOXP3$^+$ TILs in either primary breast tumors or Ax LNs is associated with an increased incidence of LN metastasis, across breast cancer subtypes (Faghih et al., 2014; Jiang et al., 2015; Kim et al., 2013; Mansfield et al., 2009; Núñez et al., 2020; van Pul et al., 2019). As 5-year survival of breast cancer patients with LN involvement is up to 40% lower than node-negative patients (Beenken et al., 2003; Dings et al., 2013), it is of crucial importance to understand the potential role of T_{regs} in the development of LN metastasis. Interestingly, one study of which we have further explored the dataset here showed that T_{regs} are not only increased in sentinel LNs with metastatic involvement but also accumulate in non-invaded sentinel LNs compared with LNs from healthy women, suggesting T_{reg} accumulation precedes LN metastasis formation (van Pul et al., 2019). Recently, others have studied the phenotype of T_{regs} in LNs of breast cancer patients and showed that T_{regs} acquire an increased effector-like phenotype in tumor cell-invaded versus non-invaded LNs (Núñez et al., 2020). These data are in line with our observations that T_{regs} in LNs are increased and activated in the context of mammary tumorigenesis. So far, clinical correlations between T_{regs} and breast cancer metastasis to other anatomical sites have not been reported, which suggest that T_{regs} may play a unique role in the formation of LN metastasis, as supported by our data.

NK cells are a well-recognized key element of the anti-tumor response (Huntington et al., 2020; López-Soto et al., 2017), but the role and cellular crosstalk of NK cells in the context of LN metastasis has remained unclear. Here, we show that NK cells in Ax TDLNs have anti-metastatic potential, provided they are relieved from the immunosuppressive pressure by T_{regs}. The relevance of these findings for human breast cancer is supported by our observation that the T_{reg}/NK cell ratio strongly shifts toward T_{regs} in SLNs of BrCa patients compared with healthy LNs. In addition, an explorative study using metastatic LNs from melanoma patients showed that *ex vivo* depletion of T_{regs} enhanced cytolytic activity of LN NK cells *in vitro*, suggesting T_{regs} can also inhibit LN NK cells in melanoma (Ghiringhelli et al., 2005). For breast cancer specifically, the expression of granzyme B within tumor-infiltrating NK cells was found to negatively correlate to T_{reg} accumulation (Mamessier et al., 2011). Furthermore, another recent study identified that clearance of Ax LN metastasis in breast cancer patients treated with neoadjuvant chemotherapy significantly correlated with increased cytotoxic potential of NK cells in peripheral blood as well as with decreased intratumoral CTLA4 gene expression (Kim et al., 2019), which is well known to be important for T_{reg} immunosuppression (Wing et al., 2008).

Our findings demonstrate that T_{regs} show tissue-dependent rewiring in response to mammary tumorigenesis, which may either be explained through tissue-specific upstream regulators or is reflective of the distinct inherent differences between tissue-resident T_{regs}, in particular in lymphoid versus non-lymphoid organs. Tissue context not only drives T_{reg} phenotype in tumor-bearing hosts but also dictates the interaction between T_{regs} and one of their cellular targets, NK cells. Specifically, we found T_{reg} depletion to differentially affect lung and LN NK cells at both the transcriptional and the protein level (Figure 5). Although transcriptomic analyses revealed that LN and lung NK cells acquire a more activated phenotype upon T_{reg} depletion, we found this to unleash NK cell-mediated anti-metastatic activity only in the LN niche, but not the lungs. We speculate that this may occur through the induction of an effector mechanism observed specifically in LN—but not lung—NK cells, such as increased expression of the cytotoxic molecules granzyme A and B, NK cell co-stimulatory receptors, or chemokine receptors (Figure 5I). Whether these specific phenotypic alterations observed in LN NK cells upon T_{reg} depletion are intrinsic to LN NK cells or due to a unique feature of tumor-educated T_{regs} in TDLNs remains to be elucidated. Alternatively, NK cells may be functionally repressed through other immunosuppressive mechanisms that are independent of T_{regs}, and specific to the lung niche. For example, we observed that lung, but not LN, NK cells undergo a shift toward a more immature state in tumor-bearing mice (Figures S5D and S5E). This occurs independent of T_{regs} and potentially affects their anti-metastatic potential. In line with this hypothesis, a recent study revealed that lung NK cells are suppressed by IL-33 activated innate lymphoid type 2 cells, which stunts their ability to control pulmonary metastasis of intravenously injected B16F10 cells (Schuijs et al., 2020). This shows that NK cells can be suppressed beyond the control of T_{regs} in the lungs, highlighting the importance of local, tissue-specific mechanisms of immunosuppression and cancer immune surveillance during metastasis formation. Finally, NK cells may be functionally irrelevant for lung metastasis formation in this model independent of their activation status, through cancer cell-intrinsic differences between lymph and lung metastasizing cancer cells that affects their likelihood to be killed by NK cells (López-Soto et al., 2017; Reiter et al., 2020), which we have not explored in this study.

The lack of T_{reg}-mediated promotion of lung metastasis formation is seemingly in contrast with studies in the 4T1 breast cancer model where T_{regs} have been shown to promote lung metastasis (Hughes et al., 2020; Liu et al., 2016). An important difference between these studies and our study is that 4T1 primary mammary tumors respond to T_{reg} depletion, resulting in attenuation of tumor growth (Hughes et al., 2020; Liu et al., 2016), while both spontaneous and transplanted primary KEP mammary tumors do not respond to T_{reg} depletion (Figures 4E and S3H). It was recently reported that the reduction in lung metastasis upon T_{reg} depletion in 4T1-bearing mice is a consequence of the primary tumor responding to T_{reg} depletion, and not an effect of T_{regs} on metastatic colonies in the lung niche (Hughes et al., 2020). In fact, an important conclusion from this study was that lung metastases are not effectively controlled after T_{reg} depletion (Hughes et al., 2020), in line with our findings that metastasis to the lungs is not influenced by T_{regs}. Furthermore, syngeneic cell lines like 4T1 poorly reflect the immunogenicity of human tumors of the same origin (Zhong et al., 2020). Recent research has shown that syngeneic cell lines derived from genetically

engineered mouse models (GEMMs) show key differences in their immune landscape, with increased frequencies of T_{regs}, $CD8^+$ T cells, and NK cells, compared with primary tumors in GEMMs (Gutierrez et al., 2021). These differences in immune landscape may critically affect the outcome of immunological studies, and thereby reduce their clinical value compared with GEMM-based models such as the KEP model.

Despite observations that exogenous IL-33 can induce acute peripheral accumulation of $ST2^+$ T_{regs} (Hemmers et al., 2021), we find that blockade of endogenous IL-33 does not affect tumor-induced systemic T_{reg} accumulation or proliferation (Figures S2F–S2I), suggesting that T_{reg} expansion in mammary tumor-bearing mice is regulated independent of IL-33, and thus remains an avenue of future research. Our *in vitro* studies (Figure S1L) suggest that a soluble factor in KEP serum can promote T_{reg} survival. An important cytokine involved in T_{reg} proliferation and survival (Sun et al., 2019b) that we did not study here is IL-2. Therefore, future studies may analyze whether IL-2 is differentially expressed or regulated in tumor-bearing hosts, and might contribute to T_{reg} expansion, as has been observed in tumor-bearing mice treated with recombinant IL-2 (Sun et al., 2019b).

In conclusion, these findings reveal a causal role for T_{regs} in the formation of LN metastasis through local suppression of NK cells, and may form the basis for the design of neo-adjuvant therapeutic strategies aimed to reduce nodal metastasis in breast cancer patients.

Limitations of the study

Although the use of a spontaneous GEMM-derived metastasis model increases the translational value of our findings, the absence of similar models for multi-organ spontaneous metastasis poses the experimental limitation of validation in comparable models. It will be relevant to extend our findings to similar models when these are generated in the future. Another possible limitation is the analysis of T_{reg} populations by bulk RNA-seq. This technique provides limited insight into changes occurring in different T_{reg} subpopulations within one tissue. Future studies may explore the distant impact of tumors on T_{regs} more deeply using single-cell RNA-seq or related techniques. Finally, we have not uncovered the molecular basis of tumor-induced T_{reg} expansion, or precise T_{reg}-NK cell interactions in the TDLN. Thus, a deeper investigation in this direction is an important avenue of future research.

STAR★METHODS

Detailed methods are provided in the online version of this paper and include the following:

SUPPLEMENTAL INFORMATION

Supplemental information can be found online at https://doi.org/10.1016/j.celrep.2022.110447.

ACKNOWLEDGMENTS

We acknowledge Alexander Rudensky for providing the IRES-DTR-GFP construct, Dr. Emiel J. Th. Rutgers and Dr. Petrousjka van den Tol for provision of clinical samples, and members of the Tumor Biology & Immunology Department, NKI, for their insightful input. We thank the flow cytometry facility, genomics core facility, animal laboratory facility, transgenesis facility, and animal pathology facility of the Netherlands Cancer Institute for technical assistance. This research was funded by NWO Oncology Graduate School Amsterdam (OOA) Diamond Program (K.K.); Netherlands Organisation for Scientific Research grant NWO-VICI 91819616 (K.E.d.V.); Dutch Cancer Society grant KWF10083, KWF10623, and KWF13191 (K.E.d.V.), KWF VU2015-7864 (R.v.d.V., T.D.d.G., K.E.d.V.); Oncode Institute (K.E.d.V.); and A Sister's Hope (T.D.d.G.). Components of the graphical abstract were prepared using Servier Medical Art, licensed under Creative Commons Attribution 3.0 Unported License.

AUTHOR CONTRIBUTIONS

K.K. and K.E.d.V. conceived the ideas and designed the experiments. K.K. performed experiments and data analysis. M.A.A. performed bioinformatical analyses. M.D.W., W.P., A.v.W., and D.D. generated data. K.K., D.K., K.V., C.-S.H., and L.R. performed animal experiments. S.A.Q. and R.B. provided a-CD25-M2A and IL33Trap, respectively. R.v.d.V., K.v.P., and T.D.d.G. collected samples and generated human data. K.E.d.V. supervised the study. K.E.d.V. and K.K. acquired funding. K.K. and K.E.d.V. wrote the paper and prepared the figures with input from all authors.

DECLARATION OF INTERESTS

K.E.d.V. reports research funding from Roche/Genentech and is a consultant for Macomics outside the scope of this work. R.v.d.V. reports research funding from Genmab. T.D.d.G. received research support from Idera Pharmaceuticals; advisory/consultancy fees from LAVA Therapeutics, Parner Therapeutics, and Immunicum; and owns stock from LAVA Therapeutics.

Received: March 23, 2021
Revised: November 1, 2021
Accepted: February 4, 2022
Published: March 1, 2022

REFERENCES

Angelova, M., Mlecnik, B., Vasaturo, A., Bindea, G., Fredriksen, T., Lafontaine, L., Buttard, B., Morgand, E., Bruni, D., Jouret-Mourin, A., et al. (2018). Evolution of metastases in space and time under immune selection. Cell *175*, 751–765.e16. https://doi.org/10.1016/j.cell.2018.09.018.

Annunziato, S., de Ruiter, J.R., Henneman, L., Brambillasca, C.S., Lutz, C., Vaillant, F., Ferrante, F., Drenth, A.P., van der Burg, E., Siteur, B., et al. (2019). Comparative oncogenomics identifies combinations of driver genes and drug targets in BRCA1-mutated breast cancer. Nat. Commun. *10*, 397. https://doi.org/10.1038/s41467-019-08301-2.

Annunziato, S., Kas, S.M., Nethe, M., Yücel, H., Del Bravo, J., Pritchard, C., Bin Ali, R., van Gerwen, B., Siteur, B., Drenth, A.P., et al. (2016). Modeling invasive lobular breast carcinoma by CRISPR/Cas9-mediated somatic genome editing of the mammary gland. Genes Dev. *30*, 1470–1480. https://doi.org/10.1101/gad.279190.116.6.

Arce Vargas, F., Furness, A.J.S., Solomon, I., Joshi, K., Mekkaoui, L., Lesko, M.H., Miranda Rota, E., Dahan, R., Georgiou, A., Sledzinska, A., et al. (2017). Fc-optimized anti-CD25 depletes tumor-infiltrating regulatory T cells and synergizes with PD-1 blockade to eradicate established tumors. Immunity *46*, 577–586. https://doi.org/10.1016/j.immuni.2017.03.013.

Aslam, M.A., Alemdehy, M.F., Hao, B., Krijger, P.H.L., Pritchard, C.E.J., De Rink, I., Muhaimin, F.I., Nurzijaha, I., van Baalen, M., Kerkhoven, R.M., et al. (2020). The Ig heavy chain protein but not its message controls early B cell development. Proc. Natl. Acad. Sci. U S A *117*, 31343–31352. https://doi.org/10.1073/pnas.2004810117.

Beenken, S.W., Urist, M.M., Zhang, Y., Desmond, R., Krontiras, H., Medina, H., and Bland, K.I. (2003). Axillary lymph node status, but not tumor size, predicts locoregional recurrence and overall survival after mastectomy for breast cancer. Ann. Surg. *237*, 732–739. https://doi.org/10.1097/01.sla.0000065289.06765.71.

Boelens, M.C., Nethe, M., Klarenbeek, S., de Ruiter, J.R., Schut, E., Bonzanni, N., Zeeman, A.L., Wientjens, E., van der Burg, E., Wessels, L., et al. (2016). PTEN loss in E-cadherin-deficient mouse mammary epithelial cells rescues apoptosis and results in development of classical invasive lobular carcinoma. Cell Rep. *16*, 2087–2101. https://doi.org/10.1016/j.celrep.2016.07.059.

Bos, P.D., Plitas, G., Rudra, D., Lee, S.Y., and Rudensky, A.Y. (2013). Transient regulatory T cell ablation deters oncogene-driven breast cancer and enhances radiotherapy. J. Exp. Med. *210*, 2435–2466. https://doi.org/10.1084/jem.20130762.

Cao, X., Cai, S.F., Fehniger, T.A., Song, J., Collins, L.I., Piwnica-Worms, D.R., and Ley, T.J. (2007). Granzyme B and perforin are important for regulatory T cell-mediated suppression of tumor clearance. Immunity *27*, 635–646. https://doi.org/10.1016/j.immuni.2007.08.014.

Chiossone, L., Chaix, J., Fuseri, N., Roth, C., Vivier, E., and Walzer, T. (2009). Maturation of mouse NK cells is a 4-stage developmental program. Blood *113*, 5488–5496. https://doi.org/10.1182/blood-2008-10-187179.

Clark, N.M., Martinez, L.M., Murdock, S., deLigio, J.T., Olex, A.L., Effi, C., Dozmorov, M.G., and Bos, P.D. (2020). Regulatory T cells support breast cancer progression by opposing IFN-γ-Dependent functional reprogramming of myeloid cells. Cell Rep. *33*, 108482. https://doi.org/10.1016/j.celrep.2020.108482.

Coffelt, S.B., Kersten, K., Doornebal, C.W., Weiden, J., Vrijland, K., Hau, C.S., Verstegen, N.J.M., Ciampricotti, M., Hawinkels, L.J.A.C., Jonkers, J., and De Visser, K.E. (2015). IL-17-producing γδ T cells and neutrophils conspire to promote breast cancer metastasis. Nature *522*, 345–348. https://doi.org/10.1038/nature14282.

Decker, T., Fischer, G., Bücke, W., Bücke, P., Stotz, F., Grüneberger, A., Gropp-Meier, M., Wiedemann, G., Pfeiffer, C., Peschel, C., and Götze, K. (2012). Increased number of regulatory T cells (T-regs) in the peripheral blood of patients with Her-2/neu-positive early breast cancer. J. Cancer Res. Clin. Oncol. *138*, 1945–1950. https://doi.org/10.1007/s00432-012-1258-3.

Derksen, P.W.B., Liu, X., Saridin, F., van der Gulden, H., Zevenhoven, J., Evers, B., van Beijnum, J.R., Griffioen, A.W., Vink, J., Krimpenfort, P., et al. (2006). Somatic inactivation of E-cadherin and p53 in mice leads to metastatic lobular mammary carcinoma through induction of anoikis resistance and angiogenesis. Cancer Cell *10*, 437–449. https://doi.org/10.1016/j.ccr.2006.09.013.

DeSantis, C.E., Ma, J., Gaudet, M.M., Newman, L.A., Miller, K.D., Goding Sauer, A., Jemal, A., and Siegel, R.L. (2019). Breast cancer statistics, 2019. CA. Cancer J. Clin. *69*, 438–451. https://doi.org/10.3322/caac.21583.

Dings, P.J.M., Elferink, M.A.G., Strobbe, L.J.A., and de Wilt, J.H.W. (2013). The prognostic value of lymph node ratio in node-positive breast cancer: a Dutch nationwide population-based study. Ann. Surg. Oncol. *20*, 2607–2614. https://doi.org/10.1245/s10434-013-2932-7.

Doornebal, C.W., Klarenbeek, S., Braumuller, T.M., Klijn, C.N., Ciampricotti, M., Hau, C.-S., Hollmann, M.W., Jonkers, J., and de Visser, K.E. (2013). A preclinical mouse model of invasive lobular breast cancer metastasis. Cancer Res. *73*, 353–363.

Duhan, V., Hamdan, T.A., Xu, H.C., Shinde, P., Bhat, H., Li, F., Al-Matary, Y., Häussinger, D., Bezgovsek, J., Friedrich, S.K., et al. (2019). NK cell–intrinsic FcεRiγ limits CD8+ T-cell expansion and thereby turns an acute into a chronic viral infection. PLoS Pathog. *15*, e1007797. https://doi.org/10.1371/journal.ppat.1007797.

Faghih, Z., Erfani, N., Haghshenas, M.R., Safaei, A., Talei, A.R., and Ghaderi, A. (2014). Immune profiles of CD4+ lymphocyte subsets in breast cancer tumor draining lymph nodes. Immunol. Lett. *158*, 57–65. https://doi.org/10.1016/j.imlet.2013.11.021.

Garner, H., and de Visser, K.E. (2020). Immune crosstalk in cancer progression and metastatic spread: a complex conversation. Nat. Rev. Immunol. *20*, 483–497. https://doi.org/10.1038/s41577-019-0271-z.

Ghiringhelli, F., Ménard, C., Terme, M., Flament, C., Taieb, J., Chaput, N., Puig, P.E., Novault, S., Escudier, B., Vivier, E., et al. (2005). CD4+CD25+ regulatory T cells inhibit natural killer cell functions in a transforming growth factor-β-dependent manner. J. Exp. Med. *202*, 1075–1085. https://doi.org/10.1084/jem.20051511.

Gómez-Cuadrado, L., Tracey, N., Ma, R., Qian, B., and Brunton, V.G. (2017). Mouse models of metastasis: progress and prospects. Dis. Model. Mech. *10*, 1061–1074. https://doi.org/10.1242/dmm.030403.

Gutierrez, W.R., Scherer, A., McGivney, G.R., Brockman, Q.R., Knepper-Adrian, V., Laverty, E.A., Roughton, G.A., and Dodd, R.D. (2021). Divergent immune landscapes of primary and syngeneic Kras-driven mouse tumor models. Sci. Rep. *11*, 1098. https://doi.org/10.1038/s41598-020-80216-1.

Hayakawa, Y., and Smyth, M.J. (2006). CD27 dissects mature NK cells into two subsets with distinct responsiveness and migratory capacity. J. Immunol. *176*, 1517–1524. https://doi.org/10.4049/JIMMUNOL.176.3.1517.

Hemmers, S., Schizas, M., and Rudensky, A.Y. (2021). T reg cell-intrinsic requirements for ST2 signaling in health and neuroinflammation. J. Exp. Med. *218*, e20201234. https://doi.org/10.1084/jem.20201234.

Holgado, A., Braun, H., Van Nuffel, E., Detry, S., Schuijs, M.J., Deswarte, K., Vergote, K., Haegman, M., Baudelet, G., Haustraete, J., et al. (2019). IL-33trap is a novel IL-33–neutralizing biologic that inhibits allergic airway inflammation. J. Allergy Clin. Immunol. *144*, 204–215. https://doi.org/10.1016/j.jaci.2019.02.028.

Hughes, E., Lauder, S.N., Smart, K., Bloom, A., Scott, J., Jones, E., Somerville, M., Browne, M., Blainey, A., Godkin, A., et al. (2020). Primary breast tumours but not lung metastases induce protective anti-tumour immune responses after Treg-depletion. Cancer Immunol. Immunother. *69*, 2063–2073. https://doi.org/10.1007/s00262-020-02603-x.

Huijbers, I.J., Del Bravo, J., Bin Ali, R., Pritchard, C., Braumuller, T.M., Van Miltenburg, M.H., Henneman, L., Michalak, E.M., Berns, A., and Jonkers, J. (2015). Using the GEMM-ESC strategy to study gene function in mouse models. Nat. Protoc. *10*, 1755–1785. https://doi.org/10.1038/nprot.2015.114.

Huntington, N.D., Cursons, J., and Rautela, J. (2020). The cancer–natural killer cell immunity cycle. Nat. Rev. Cancer *20*, 437–454. https://doi.org/10.1038/s41568-020-0272-z.

Jiang, D., Gao, Z., Cai, Z., Wang, M., and He, J. (2015). Clinicopathological and prognostic significance of FOXP3+ tumor infiltrating lymphocytes in patients with breast cancer: a meta-analysis. BMC Cancer *15*, 727. https://doi.org/10.1186/s12885-015-1742-7.

Kim, J.M., Rasmussen, J.P., and Rudensky, A.Y. (2007). Regulatory T cells prevent catastrophic autoimmunity throughout the lifespan of mice. Nat. Immunol. *8*, 191–197. https://doi.org/10.1038/ni1428.

Kim, R., Kawai, A., Wakisaka, M., Funaoka, Y., Yasuda, N., Hidaka, M., Morita, Y., Ohtani, S., Ito, M., and Arihiro, K. (2019). A potential role for peripheral natural killer cell activity induced by preoperative chemotherapy in breast cancer patients. Cancer Immunol. Immunother. *68*, 577–585. https://doi.org/10.1007/s00262-019-02305-z.

Kim, S.T., Jeong, H., Woo, O.H., Seo, J.H., Kim, A., Lee, E.S., Shin, S.W., Kim, Y.H., Kim, J.S., and Park, K.H. (2013). Tumor-infiltrating lymphocytes, tumor characteristics, and recurrence in patients with early breast cancer. Am. J. Clin. Oncol. Cancer Clin. Trials *36*, 224–231. https://doi.org/10.1097/COC.0b013e3182467d90.

Kos, K., and de Visser, K.E. (2021). The multifaceted role of regulatory T cells in breast cancer. Annu. Rev. Cancer Biol. *5*, 291–310. https://doi.org/10.1146/annurev-cancerbio-042920-104912.

Kos, K., van Baalen, M., Meijer, D.A., and de Visser, K.E. (2019). Flow cytometry-based isolation of tumor-associated regulatory T cells and assessment of their suppressive potential. Methods Enzymol. *632*, 259–281. https://doi.org/10.1016/bs.mie.2019.07.035.

Lambert, A.W., Pattabiraman, D.R., and Weinberg, R.A. (2017). Emerging biological principles of metastasis. Cell *168*, 670–691. https://doi.org/10.1016/j.cell.2016.11.037.

Li, A., Herbst, R.H., Canner, D., Schenkel, J.M., Smith, O.C., Kim, J.Y., Hillman, M., Bhutkar, A., Cuoco, M.S., Rappazzo, C.G., et al. (2019). IL-33 signaling alters regulatory T cell diversity in support of tumor development. Cell Rep. *29*, 2998–3008.e8. https://doi.org/10.1016/j.celrep.2019.10.120.

Liberzon, A., Birger, C., Thorvaldsdóttir, H., Ghandi, M., Mesirov, J.P., and Tamayo, P. (2015). The molecular signatures database hallmark gene set collection. Cell Syst. *1*, 417–425. https://doi.org/10.1016/j.cels.2015.12.004.

Liu, J., Blake, S.J., Yong, M.C.R., Harjunpää, H., Ngiow, S.F., Takeda, K., Young, A., O'Donnell, J.S., Allen, S., Smyth, M.J., and Teng, M.W.L. (2016). Improved efficacy of neoadjuvant compared to adjuvant immunotherapy to eradicate metastatic disease. Cancer Discov. *6*, 1382–1399. https://doi.org/10.1158/2159-8290.CD-16-0577.

Liu, S., Foulkes, W.D., Leung, S., Gao, D., Lau, S., Kos, Z., and Nielsen, T.O. (2014). Prognostic significance of FOXP3+ tumor-infiltrating lymphocytes in breast cancer depends on estrogen receptor and human epidermal growth factor receptor-2 expression status and concurrent cytotoxic T-cell infiltration. Breast Cancer Res. *16*, 432. https://doi.org/10.1186/s13058-014-0432-8.

Liyanage, U.K., Moore, T.T., Joo, H.-G., Tanaka, Y., Herrmann, V., Doherty, G., Drebin, J.A., Strasberg, S.M., Eberlein, T.J., Goedegebuure, P.S., and Linehan, D.C. (2002). Prevalence of regulatory T cells is increased in peripheral blood and tumor microenvironment of patients with pancreas or breast adenocarcinoma. J. Immunol. *169*, 2756–2761. https://doi.org/10.4049/jimmunol.169.5.2756.

López-Soto, A., Gonzalez, S., Smyth, M.J., and Galluzzi, L. (2017). Control of metastasis by NK cells. Cancer Cell *32*, 135–154. https://doi.org/10.1016/j.ccell.2017.06.009.

Magnuson, A.M., Kiner, E., Ergun, A., Park, J.S., Asinovski, N., Ortiz-Lopez, A., Kilcoyne, A., Paoluzzi-Tomada, E., Weissleder, R., Mathis, D., and Benoist, C. (2018). Identification and validation of a tumor-infiltrating Treg transcriptional signature conserved across species and tumor types. Proc. Natl. Acad. Sci. U S A *115*, E10672–E10681. https://doi.org/10.1073/pnas.1810580115.

Mamessier, E., Sylvain, A., Thibult, M.L., Houvenaeghel, G., Jacquemier, J., Castellano, R., Gonçalves, A., André, P., Romagné, F., Thibault, G., et al. (2011). Human breast cancer cells enhance self tolerance by promoting evasion from NK cell antitumor immunity. J. Clin. Invest. *121*, 3609–3622. https://doi.org/10.1172/JCI45816.

Mansfield, A.S., Heikkila, P.S., Vaara, A.T., von Smitten, K.A.J., Vakkila, J.M., and Leidenius, M.H.K. (2009). Simultaneous Foxp3 and Ido expression is associated with sentinel lymph node metastases in breast cancer. BMC Cancer *9*. https://doi.org/10.1186/1471-2407-9-231.

Matta, B.M., and Turnquist, H.R. (2016). Expansion of regulatory T cells *in vitro* and *in vivo* by IL-33. In Methods in Molecular Biology (Humana Press Inc.), pp. 29–41. https://doi.org/10.1007/978-1-4939-3139-2_3.

Núñez, N.G., Tosello Boari, J., Ramos, R.N., Richer, W., Cagnard, N., Anderfuhren, C.D., Niborski, L.L., Bigot, J., Meseure, D., De La Rochere, P., et al. (2020). Tumor invasion in draining lymph nodes is associated with Treg accumulation in breast cancer patients. Nat. Commun. *11*, 1–15. https://doi.org/10.1038/s41467-020-17046-2.

Pastille, E., Wasmer, M.H., Adamczyk, A., Vu, V.P., Mager, L.F., Phuong, N.N.T., Palmieri, V., Simillion, C., Hansen, W., Kasper, S., et al. (2019). The IL-33/ST2 pathway shapes the regulatory T cell phenotype to promote intestinal cancer. Mucosal Immunol. *12*, 990–1003. https://doi.org/10.1038/s41385-019-0176-y.

Paul, S., and Lal, G. (2017). The molecular mechanism of natural killer cells function and its importance in cancer immunotherapy. Front. Immunol. *8*, 1124. https://doi.org/10.3389/FIMMU.2017.01124.

Perez, S.A., Karamouzis, M.V., Skarlos, D.V., Ardavanis, A., Sotiriadou, N.N., Iliopoulou, E.G., Salagianni, M.L., Orphanos, G., Baxevanis, C.N., Rigatos, G., and Papamichail, M. (2007). CD4+CD25+ regulatory T-cell frequency in HER-2/neu (HER)-Positive and HER-negative advanced-stage breast cancer patients. Clin. Cancer Res. *13*, 2714–2721. https://doi.org/10.1158/1078-0432.CCR-06-2347.

Picelli, S., Faridani, O.R., Björklund, Å.K., Winberg, G., Sagasser, S., and Sandberg, R. (2014). Full-length RNA-seq from single cells using Smart-seq2. Nat. Protoc. *9*, 171–181. https://doi.org/10.1038/nprot.2014.006.

Plitas, G., Konopacki, C., Wu, K., Bos, P.D., Morrow, M., Putintseva, E.V., Chudakov, D.M., and Rudensky, A.Y. (2016). Regulatory T cells exhibit distinct features in human breast cancer. Immunity *45*, 1122–1134. https://doi.org/10.1016/j.immuni.2016.10.032.

Plitas, G., and Rudensky, A.Y. (2020). Regulatory T cells in cancer. Annu. Rev. Cancer Biol. *4*, 459–477. https://doi.org/10.1146/annurev-cancerbio-030419-033428.

Poli, A., Michel, T., Thérésine, M., Andrès, E., Hentges, F., and Zimmer, J. (2009). CD56bright natural killer (NK) cells: an important NK cell subset. Immunology *126*, 458–465. https://doi.org/10.1111/j.1365-2567.2008.03027.x.

Reiter, J.G., Hung, W.T., Lee, I.H., Nagpal, S., Giunta, P., Degner, S., Liu, G., Wassenaar, E.C.E., Jeck, W.R., Taylor, M.S., et al. (2020). Lymph node metastases develop through a wider evolutionary bottleneck than distant metastases. Nat. Genet. *52*, 692–700. https://doi.org/10.1038/s41588-020-0633-2.

Schuijs, M.J., Png, S., Richard, A.C., Tsyben, A., Hamm, G., Stockis, J., Garcia, C., Pinaud, S., Nicholls, A., Ros, X.R., et al. (2020). ILC2-driven innate immune checkpoint mechanism antagonizes NK cell antimetastatic function in the lung. Nat. Immunol. *21*, 998–1009. https://doi.org/10.1038/s41590-020-0745-y.

Son, J., Cho, J.-W., Park, H.J., Moon, J., Park, S., Lee, H., Lee, J., Kim, G., Park, S.M., Lira, S.A., et al. (2020). Tumor-infiltrating regulatory T cell accumulation in the tumor microenvironment is mediated by IL33/ST2 signaling. Cancer Immunol. Res. *8*, 1393–1406. https://doi.org/10.1158/2326-6066.cir-19-0828.

Subramanian, A., Tamayo, P., Mootha, V.K., Mukherjee, S., Ebert, B.L., Gillette, M.A., Paulovich, A., Pomeroy, S.L., Golub, T.R., Lander, E.S., and Mesirov, J.P. (2005). Gene set enrichment analysis: a knowledge-based approach for interpreting genome-wide expression profiles. Proc. Natl. Acad. Sci. U S A *102*, 15545–15550. https://doi.org/10.1073/pnas.0506580102.

Sun, L., Dong, S., Ge, Y., Fonseca, J.P., Robinson, Z.T., Mysore, K.S., and Mehta, P. (2019a). DiVenn: an interactive and integrated web-based visualization tool for comparing gene lists. Front. Genet. *10*, 421. https://doi.org/10.3389/fgene.2019.00421.

Sun, Z., Ren, Z., Yang, K., Liu, Z., Cao, S., Deng, S., Xu, L., Liang, Y., Guo, J., Bian, Y., et al. (2019b). A next-generation tumor-targeting IL-2 preferentially promotes tumor-infiltrating CD8+ T-cell response and effective tumor control. Nat. Commun. *10*, 3874. https://doi.org/10.1038/S41467-019-11782-W.

van Pul, K.M., Vuylsteke, R.J.C.L.M., van de Ven, R., te Velde, E.A., Rutgers, E.J.T., van den Tol, P.M., Stockmann, H.B.A.C., and de Gruijl, T.D. (2019). Selectively hampered activation of lymph node-resident dendritic cells precedes profound T cell suppression and metastatic spread in the breast cancer sentinel lymph node. J. Immunother. Cancer *7*, 133. https://doi.org/10.1186/s40425-019-0605-1.

Vuylsteke, R.J.C.L.M., Van Leeuwen, P.A.M., Meijer, S., Wijnands, P.G.J.T.B., Muller, M.G.S., Busch, D.H., Scheper, R.J., and De Gruijl, T.D. (2002). Sampling tumor-draining lymph nodes for phenotypic and functional analysis of dendritic cells and T cells. Am. J. Pathol. *161*, 19–26. https://doi.org/10.1016/S0002-9440(10)64152-1.

Wang, L., Simons, D.L., Lu, X., Tu, T.Y., Solomon, S., Wang, R., Rosario, A., Avalos, C., Schmolze, D., Yim, J., et al. (2019). Connecting blood and intratumoral Treg cell activity in predicting future relapse in breast cancer. Nat. Immunol. *20*, 1220–1230. https://doi.org/10.1038/s41590-019-0429-7.

Wellenstein, M.D., Coffelt, S.B., Duits, D.E.M., van Miltenburg, M.H., Slagter, M., de Rink, I., Henneman, L., Kas, S.M., Prekovic, S., Hau, C.S., et al. (2019). Loss of p53 triggers WNT-dependent systemic inflammation to drive breast cancer metastasis. Nature *572*, 538–542. https://doi.org/10.1038/s41586-019-1450-6.

Wing, K., Onishi, Y., Prieto-Martin, P., Yamaguchi, T., Miyara, M., Fehervari, Z., Nomura, T., and Sakaguchi, S. (2008). CTLA-4 control over Foxp3+ regulatory T cell function. Science *322*, 271–275. https://doi.org/10.1126/science.1160062.

Wolf, A.M., Wolf, D., Steurer, M., Gastl, G., Gunsilius, E., and Grubeck-Loebenstein, B. (2003). Increase of regulatory T cells in the peripheral blood of cancer patients. Clin. Cancer Res. *9*, 606–612.

Zhong, W., Myers, J.S., Wang, F., Wang, K., Lucas, J., Rosfjord, E., Lucas, J., Hooper, A.T., Yang, S., Lemon, L.A., et al. (2020). Comparison of the molecular and cellular phenotypes of common mouse syngeneic models with human tumors. BMC Genomics *21*, 2. https://doi.org/10.1186/s12864-019-6344-3.

STAR★METHODS

KEY RESOURCES TABLE

REAGENT or RESOURCE	SOURCE	IDENTIFIER
Antibodies		
Armenian Hamster anti-CD3e, APC (clone 145-2C11)	Invitrogen	#Cat 17-0031-82
Armenian Hamster anti-CD3e, FITC (clone 145-2C11)	Biolegend	#Cat 100306
Armenian Hamster anti-CD3e, PE-Cy7 (clone 145-2C11)	eBioscience	#Cat 25-0031-82
Armenian Hamster anti-CD3e, PE (clone 145-2C11)	Biolegend	#Cat 100307
Rat anti-CD4, BV421 (clone GK1.5)	BD	#Cat 562891
Rat anti-CD4, BUV805 (clone GK1.5)	BD	#Cat 612900
Rat anti-CD4, PE (clone GK1.5)	Invitrogen	#Cat 12-0041-82
Rat anti-CD8, AF700 (clone 56-6.7)	BioLegend	#Cat 100730
Rat anti-CD8, BUV395 (clone 56-6.7)	BD	#Cat 563786
Rat anti-CD8, FITC (clone 56-6.7)	eBioscience	#Cat 11-0081-85
Rat anti-CD11b, APC (clone M1/70)	eBioscience	#Cat 17-01120-82
Rat anti-CD11b, BV786 (clone M1/70)	BD	#Cat 740861
Rat anti-CD25, PE (clone PC61)	Biolegend	#Cat 102008
Rat anti-CD25, APC (clone PC61)	Biolegend	#Cat 102011
Armenian Hamster anti-CD27, PerCP-eFluor 710 (clone LG.7F9)	ThermoFisher	#Cat 46-0271-82
Rat anti-CD44, BV605 (clone IM7)	Biolegend	#Cat 103047
Rat anti-CD45, BUV395 (clone 30F11)	BD	#Cat 564279
Rat anti-CD45, BUV563 (clone 30F11)	BD	#Cat 612924
Rat anti-CD45, APC-eF780 (clone 30F11)	eBioscience	#Cat 47-0451-82
Rat anti-CD49b, eF450 (clone DX5)	ThermoFisher	#Cat 48-5971-82
Rat anti-CD62L, AF700 (clone MEL-14)	ThermoFisher	#Cat 56-0621-82
Hamster anti-CD69, BUV737 (clone H1.2F3)	BD	#Cat 612793
Rat anti-CD103, BV711 (clone M290)	BD	#Cat 564320
Rat anti-mouse CD107a, PE (clone 1D4B)	Biolegend	#Cat 121611
Armenian hamster anti-CD152, PE-Cy7 (clone UC10-4B9)	Biolegend	#Cat 106313
Armenian hamster anti-CD278, PerCP-Cy5.5 (clone C398.4A)	Biolegend	#Cat 313517
Mouse anti-FOXP3, AF647 (clone 150D)	Biolegend	#Cat 320014
Mouse anti-Granzyme B, PE (clone QA16A02)	Biolegend	#Cat 372208
Rat anti-IFNy, eF450 (clone XMG1.2)	ThermoFisher	#Cat 48-7311-82
Rat anti-Ki67, PE (clone SOL-A15)	ThermoFisher	#Cat 12-5698-80
Mouse anti Ki-67, BV786 (clone B56)	BD	#Cat 563756
Mouse anti-NK1.1, APC-eFluor 780 (clone PK136)	ThermoFisher	#Cat 47-5941-82
Rat anti-NKp46, FITC (clone 29A1.4)	ThermoFisher	#Cat 11-3351-82
Rat anti-ST2, PE (clone RMST2-2)	ThermoFisher	#Cat 12-9335-82
Rat anti-TNFa, AF700 (clone MP6-XT22)	Biolegend	#Cat 506338
anti-CD25, mIgG2a (clone M2A)	Gift from S. Quezada (under MTA), produced by Evitria	N/A

(*Continued on next page*)

Continued

REAGENT or RESOURCE	SOURCE	IDENTIFIER
Mouse IgG2a isotype control (clone C1.18.4)	BioXcell	#Cat BE0085
InVivoPlus anti-mouse CD8α (clone 2.43)	BioXcell	#Cat BP0061
InVivoPlus anti-mouse NK1.1 (clone PK136)	BioXcell	#Cat BP0036
Purified Hamster Anti-Mouse CD3e	BD	#Cat 553058
Goat anti-IL-33 (polyclonal)	R&D Systems	#Cat AF3626
Goat IgG control (polyclonal)	R&D Systems	#Cat AB-108-C
Rat anti-Keratine-8 (TROMA I)	DSHB University of Iowa	#Cat Troma I
Rabbit anti-E-Cadherin (24E10)	Cell Signaling	#Cat 3195
Rat Anti-Mouse CD16/CD32, purified (clone 2.4G2)	BD	#Cat 553141
Armenian Hamster anti-CD3e, purified (clone 145-2C11)	Biolegend	#Cat 100302
Mouse anti-human CD3, APC (clone SK7)	BD	#Cat 340661
Mouse anti-human CD3, PerCP-cy5.5 (clone SK7)	BD	#Cat 340949
Mouse anti-human CD56, PE (clone B159)	BD	#Cat 561903
Mouse anti-human CD16, FITC (clone 3G8)	BD	#Cat 555406
Mouse anti-human IgG1, FITC (clone X40)	BD	#Cat 345815
Mouse anti-human CD25, APC (2A3)	BD	#Cat 340939
Mouse anti-human FoxP3, PE (PCH101)	ThermoFisher	#Cat 12-4776-42
Bacterial and virus strains		
pLenti#737-P2A-Cre	Gift from Jos Jonkers (NKI)	N/A
Biological samples		
KEP tumor fragments	This paper	N/A
Chemicals, peptides, and recombinant proteins		
Dynabeads mouse T-activator CD3/CD28	Thermofisher	#Cat 11452D
Recombinant murine IL-2	Peprotech	#Cat 212-12
7-AAD Viability Staining Solution	Thermofisher	#Cat 00-6993-50
Ionomycin (calcium salt from Streptomyces conglobatus)	Sigma	#Cat I0634-1mg
Phorbol 12-myristate 13-acetate (PMA)	Sigma	#Cat P1585-1MG
UltraComp eBeads	eBioscience	#Cat 01-2222-42
DNAse I	Invitrogen	#Cat 18068-015
Collagenase A	Roche	#Cat 11088793001
BD Brilliant stain buffer	BD	#Cat 563794
Liberase TL Research Grade	Roche	#Cat 5401020001
Diphtheria Toxin from Corynebacterium diphtheriae	Sigma-Aldrich	#Cat D0564-1MG
RLT Buffer	Qiagen	#Cat 79216
5-Ethynyl-2'-deoxyuridine	Sigma	#Cat 900584-50MG
GolgiStop	BD	#Cat 554724
GolgiPlug	BD	#Cat 555029
IL-33 Trap	Gift from Rudi Beyaert, VIB (under MTA)	N/A
Critical commercial assays		
LEGENDplex™ Mouse IL-33 Capture Bead B5, 13X	Biolegend	#Cat 740144
LEGENDplex™ Mouse Cytokine Panel 2 Standard	Biolegend	#Cat 740372
LEGENDplex™ Mouse Cytokine Panel 2 Detection Antibodies	Biolegend	#Cat 740149
LEGENDplex™ Buffer Set B	Biolegend	#Cat 740373

(*Continued on next page*)

Continued

REAGENT or RESOURCE	SOURCE	IDENTIFIER
LIVE/DEAD™ Fixable Near-IR Dead Cell Stain Kit	ThermoFisher	#Cat L34975
LIVE/DEAD™ Fixable Aqua Dead Cell Stain Kit	ThermoFisher	#Cat L34957
Zombie Red™ Fixable Viability Kit	Biolegend	#Cat 423109
Zombie NIR™ Fixable Viability Kit	Biolegend	#Cat 423105
CellTrace™ Violet Cell Proliferation Kit	ThermoFisher	#Cat C34557
Click-iT™ EdU Cell Proliferation Kit for Imaging, Alexa Fluor™ 488 dye	ThermoFisher	#Cat C10337
Foxp3/Transcription Factor Staining Buffer Set	ThermoFisher	#Cat 00-5523-00
Deposited data		
Raw and analyzed data (Treg RNAseq)	This paper	GEO: GSE169024
Raw and analyzed data (NK RNAseq)	This paper	GEO: GSE169025
Experimental Models: Organisms/Strains		
Mus musculus: Strain: Wild-type FVB/N	Janvier Laboratories	FVB/N
Mus musculus: Strain: *K14-cre; Cdh1$^{F/F}$;Trp53$^{F/F}$* (FVB/n)	Netherlands Cancer Institute	N/A
Mus musculus: Strain *Wap-cre; Cdh1$^{F/F}$;Pik3ca^{E545K}* (FVB/n)	Netherlands Cancer Institute	N/A
Mus musculus: Strain *Wap-cre; Cdh1$^{F/F}$;Akt^{E17K}* (FVB/n)	Netherlands Cancer Institute	N/A
Mus musculus: Strain *Cdh1$^{F/F}$; Trp53$^{F/F}$;Foxp3$^{GFP\text{-}DTR}$*(FVB/n)	Netherlands Cancer Institute	N/A
Mus musculus: Strain *Wap-cre; Cdh1$^{F/F}$;Pten$^{F/F}$* (FVB/n)	Netherlands Cancer Institute	N/A
Mus musculus: Strain *Wap-cre; Cdh1$^{F/F}$;Pik3ca^{H1047R}* (FVB/n)	Netherlands Cancer Institute	N/A
Mus musculus: Strain *Brca1$^{F/F}$; Trp53$^{F/F}$* (FVB/n)	Netherlands Cancer Institute	N/A
Recombinant DNA		
Plasmid: IRES-DTR-GFP	Gift from Alexander Rudensky (MSKCC)	N/A
Software and algorithms		
FlowJo v10.7	https://www.flowjo.com/solutions/flowjo	N/A
GSEA v4.0.3	https://www.gsea-msigdb.org/gsea/index.jsp	N/A
R statistical programming environment	R Foundation for Statistical Computing	https://www.r-project.org
GraphPad Prism v8	https://www.graphpad.com/scientific-software/prism/	N/A
G*power software v3.1	https://www.psychologie.hhu.de/arbeitsgruppen/allgemeine-psychologie-und-arbeitspsychologie/gpower.html	N/A
Tophat 2.1.0	https://ccb.jhu.edu/software/tophat/index.shtml	N/A
Itreecount	(https://github.com/NKI-GCF/itreecount)	N/A
Hisat2	http://daehwankimlab.github.io/hisat2/	N/A

RESOURCE AVAILABILITY

Lead contact

Further information and requests for resources and reagents should be directed to and will be fulfilled by the lead contact, Karin. E. de Visser (K.d.visser@nki.nl).

Materials availability

All reagents generated in this study are available upon request with a completed material transfer agreement.

Data and code availability

Bulk T_{reg} and NK RNA-sequencing data have been deposited in the GEO and are publicly available as of the date of publication. Accession numbers are listed in the key resources table.

This paper does not report original code.

Any additional information required to reanalyze the data reported in this paper is available from the lead contact upon request.

EXPERIMENTAL MODEL AND SUBJECT DETAILS

Mice

The generation and characterization of genetically engineered mouse models for spontaneous mammary tumorigenesis has been described before (Annunziato et al., 2016, 2019; Boelens et al., 2016; Derksen et al., 2006; Wellenstein et al., 2019). The following mice have been used in this study: Keratin14 (*K14)-cre;Cdh1*$^{F/F}$*;Trp53*$^{F/F}$, Whey Acidic Protein (*Wap)-cre;Cdh1*$^{F/F}$*;Pik3ca*^{E545K}, *(Wap)-cre;Cdh1*$^{F/F}$*;Pik3ca*^{H1047R}, *Wap-cre;Cdh1*$^{F/F}$*;Pten*$^{F/F}$, *Wap-cre;Cdh1*$^{F/F}$*;Akt*^{E17K}, *Brca1*$^{F/F;}$*Trp53*$^{F/F}$ (generous gift of Jos Jonkers, NKI) and *Cdh1*$^{F/F}$*;Trp53*$^{F/F}$*;Foxp3*$^{GFP\text{-}DTR}$ mice (further referred to as *Foxp3*$^{GFP\text{-}DTR}$). All mouse models were on FVB/n background, and genotyping was performed by PCR analysis on toe clips DNA as described (Derksen et al., 2006). Starting at 6–7 weeks of age, female mice were monitored twice weekly for the development of spontaneous mammary tumor development. Tumors in *Brca1*$^{F/F}$*;Trp53*$^{F/F}$ mice were somatically induced through intraductal delivery of lentiviral-Cre as described before (Annunziato et al., 2019, 2016). Mice were monitored twice weekly for spontaneous mammary tumor development starting 6 weeks after intraductal delivery of lenti-viral Cre. Upon mammary tumor formation, perpendicular tumor diameters were measured twice weekly using a caliper. In all models, end-stage was defined as cumulative tumor burden of 225mm^2. Age-matched WT littermates were used as controls.

Mice were kept in individually ventilated cages at the animal laboratory facility of the Netherlands Cancer Institute under specific pathogen free conditions. Food and water were provided *ad libitum.* All animal experiments were approved by the Netherlands Cancer Institute Animal Ethics Committee, and performed in accordance with institutional, national and European guidelines for Animal Care and Use. The study is compliant with all relevant ethical regulations regarding animal research.

Patients

The mean age of the ten female patients at the time of SLN procedure was 56.3 years. Patients had either lobular (n = 2) or ductal (n = 6) carcinoma of the breast, one patient had a tumor that was classified as ductal/lobular and one patient a tumor that was classified as mucinous adenocarcinoma. One patient, who was diagnosed with two invasive breast tumors (ductal), had both a luminal A (Her2-, ER+, PR+) and a luminal B Her2+ (Her2+, ER-, PR-) tumor. All other patients were diagnosed with hormone receptor expressing (Her2-, ER+, PR+) tumors, of which six were classified as luminal A and three as luminal B. The study was approved by the Institutional Review Board (IRB) of the VU University medical center and SLN samples were collected and handled according to guidelines described in the Code of Conduct for Proper Use of Human Tissue of the Dutch Federation of Biomedical Scientific Societies with written informed consent from the patients prior to SLN sampling.

METHOD DETAILS

Generation of Foxp3$^{GFP\text{-}DTR}$ mice

Cdh1$^{F/F}$*;Trp53*$^{F/F}$*;Foxp3*$^{GFP\text{-}DTR}$ mice (further referred to as *Foxp3*$^{GFP\text{-}DTR}$) were generated using the previously described IRES-DTR-GFP targeting construct (Kim et al., 2007) (generous gift of Prof. Alexander Rudensky, MSKCC). Notably, Cre-recombinase is not expressed in *Foxp3*$^{GFP\text{-}DTR}$ mice, and generation of *Foxp3*$^{GFP\text{-}DTR}$ mice within the *Cdh1*$^{F/F}$;*Trp53*$^{F/F}$ background matches the background of control (*Cdh1*$^{F/F}$;*Trp53*$^{F/F}$) mice used throughout the manuscript. The linearized IRES-DTR-GFP construct was introduced in the 3′ untranslated region of Foxp3 upstream of the polyadenylation signal in *Cdh1*$^{F/F}$;*Trp53*$^{F/F}$ (FVB) embryonic stem cells (ESC) by electroporation as described before (Huijbers et al., 2015; Kim et al., 2007). Neomycin-resistant clones were screened by PCR across the 3' arm. Correct targeting of the construct was confirmed by Southern blot. Correctly targeted clones were transfected with a FLP-deleter plasmid for excision of the PGK-Neo cassette. Transfected clones were selected by puromycin, and loss of the PGK-Neo cassette was confirmed by PCR. Selected ESCs were injected into C57BL/6N blastocysts and chimeric male offspring were mated to *Cdh1*$^{F/F}$;*Trp53*$^{F/F}$ mice. Homozygous *Cdh1*$^{F/F}$*;Trp53*$^{F/F}$*;Foxp3*$^{GFP\text{-}DTR}$ females were used for experiments.

KEP metastasis model

The KEP metastasis model has been applied as previously described (Doornebal et al., 2013). Tumors from KEP mice (100mm^2) were fragmented into small pieces (~1 mm^2) and stored at -150°C in Dulbecco's Modified Eagle's Medium F12 containing 30% fetal calf serum and 10% dimethyl sulfoxide. Selection of mouse invasive lobular carcinomas (mILC) donor tumors was based on high cytokeratin 8 and absence of vimentin and E-cadherin expression as determined by immunohistochemistry. Donor KEP tumor pieces were orthotopically transplanted into the 4th mammary fat pad of female recipient 9–12 week old WT FVB/n mice (Janvier). Upon tumor outgrowth to a size of 100mm^2, donor tumors were surgically removed. Following mastectomy, mice were monitored for development of overt multi-organ metastatic disease by daily palpation and observation of physical health, appearance, and behavior.

Lungs, liver, spleen, intestines, mesenterium, kidneys, adrenal glands, and tumor-draining (subiliac, proper axillary and accessory axillary) and distant LNs (mesenteric, renal, and caudal) were collected and analyzed microscopically for the presence of metastatic foci by immunohistochemical cytokeratin 8 staining. Macroscopically overt metastases were collected separately for further analysis. Mice were excluded from analysis due to following predetermined reasons: No outgrowth of tumors upon transplantation, mice sacrificed due to surgery-related complications, mice sacrificed due to development of end-stage ($225mm^2$) local recurrent tumors prior to presentation of metastatic disease.

Murine intervention studies

Antibody treatments were initiated at tumor sizes of 25–$45mm^2$ (as indicated) in spontaneous mammary tumor-bearing KEP and *Foxp3*$^{GFP\text{-}DTR}$ mice, and at 12–$20mm^2$ in the KEP metastasis model (neo-adjuvant setting). Mice were randomly allocated to treatment groups upon presentation of mammary tumors of indicated size. Tumor development in KEP mice prevented full blinding to genotypes during mouse handling, but researchers were blinded to treatment and genotype during cell, tissue and immunohistological analysis. Mice were intraperitoneally injected with: Fc-receptor optimized anti-CD25 (Clone M2a (Arce Vargas et al., 2017) 200 μg weekly for 2 weeks; mIgG2a control antibody 200 μg weekly for 2 weeks (C1.18.4, BioXcell); anti-mouse CD8α single loading dose of 400 μg, followed by 200 μg thrice a week (2.43, BioXcell); anti-mouse NK1.1, single loading dose of 400 μg, followed by 200 μg twice a week (PK136, BioXcell); Difteria Toxin (Sigma) 25 μg twice total (t = 0, t = 7 days); anti-mouse IL-33 (R&D systems) 3.75 μg thrice a week for 2 weeks; IL-33Trap (Holgado et al., 2019) 50 μg daily for 1 week. Animal sample size for intervention studies was determined by power analysis using G*power software, using effect sizes obtained from historical experiments or preliminary data. Due to the spontaneous nature of the used animal models for primary tumor formation and metastasis, cohorts were sequentially completed and analyzed in succession, similar in set up to clinical trials. In the KEP metastasis model, treatments were discontinued upon mastectomy. For survival curve experiments and end-stage analyses in KEP mice, antibody treatment continued until the tumor or the cumulative tumor burden reached $225mm^2$. For KEP intervention and KEP metastasis experiments, the following end points were applied according to the Code of Practice Animal Experiments in cancer research: (metastatic) tumor size >$225mm^2$, >20% weight loss since start of experiment, respiratory distress upon fixation, severe lethargy, (metastatic) tumor causing severe clinical symptoms as a result of location, invasive growth or ulceration.

Preparation of single cell suspensions

For flow cytometry based analysis and cell sorting for *in vitro* assays and RNA sequencing, single cell suspensions were prepared from freshly isolated mouse tissues. Mice were sacrificed at indicated time points. KEP tumors, healthy mammary glands spleens and LNs were prepared as previously described (Kos et al., 2019). In brief, tumors and mammary glands were mechanically chopped using the McIlwain tissue chopper (Mickle Laboratory Engineering) and enzymatically digested with 3 mg/ml collagenase type A (Roche) and 25 μg/ml DNase I (Sigma) in serum-free medium for 1 h at 37°C in a shaking water bath. Enzyme activity was neutralized by addition of cold DMEM/8% FCS and suspension was dispersed through a 70 μm cell strainer. Lungs were perfused with ice-cold PBS *post mortem* to flush blood. Next, lungs were cut into small pieces and mechanically chopped using the McIlwain tissue chopper. Lungs were enzymatically digested in 100 μg/mL Liberase Tm (Roche) under continuous rotation for 30 minutes at 37°C. Enzyme activity was neutralized by addition of cold DMEM/8% FCS and suspension was dispersed through a 70 μm cell strainer. Spleens and lymph nodes were collected in ice-cold PBS, and dispersed through a 70 μm cell strainer. Blood was obtained via cardiac puncture for end-stage analyses, and via tail vein puncture for time point analyses and collected in tubes containing heparin. Erythrocyte lysis for blood, spleen and lungs was performed using NH_4Cl erythrocyte lysis buffer for 2x5 (blood) and 1x1 (spleen, lungs) minutes.

Flow cytometry: analysis and cell sorting

Single cell suspensions of human and murine samples were incubated in anti-CD16/32 (2.4G2, BD Biosciences) to block unspecific Fc receptor binding for 5 minutes. Next, cells were incubated for 20 minutes with fluorochrome conjugated antibodies diluted in FACS buffer (2.5% FBS, 2 mM EDTA in PBS). For analysis of nuclear transcription factors, cells were fixed and permeabilized after surface and live/dead staining using the FOXP3 Transcription buffer set (Thermofisher), according to manufacturer's instruction. Fixation permeabilization and intracellular FOXP3 staining was performed for 30 minutes. For analysis of granzyme B, TNFα and IFNy, single cell suspensions were incubated in cIMDM (IMDM containing 8% FCS, 100 IU/ml penicillin, 100 μg/ml streptomycin, 0.5% β-mercaptoethanol), 50 ng/ml PMA, 1 μM ionomycin and Golgi-Plug (1:1000; BD Biosciences) for 3 h at 37°C prior to surface staining. For analysis of T_{reg} proliferation *in vivo*, mice were injected with the thymidine analog EdU (200 μg) 24 and 48h prior to sacrifice. DNA incorporation of EdU was measured using Click-iT^{TM} EdU Cell Proliferation Kit for Imaging according to manufacturer's instruction. Cell suspensions were analyzed on a BD LSR2 SORP or BD Symphony SORP, or sorted on a FACS ARIA II (4 lasers), or FACS FUSION (5 lasers). Single cell suspensions for cell sorting were prepared under sterile conditions. Gating strategies for T_{reg} sorting as previously described (Kos et al., 2019). See key resources table for antibodies used. Absolute cell counts were determined using 123count eBeads (ThermoFisher) according to manufacturer's instruction.

T_{reg} suppression assays

T_{reg}-T cell suppression assays were performed as previously described (Kos et al., 2019). Briefly, T_{regs} (Live, $CD45^+$, $CD3^+$, $CD8^-$ $CD4^+$, $CD25^{high}$) sorted from freshly isolated samples were activated overnight in IMDM containing 8% FCS, 100 IU/ml penicillin,

100 μg/ml streptomycin, 0.5% β-mercapto-ethanol, 300U/mL IL-2, 1:5 bead:cell ratio CD3/CD28 coated beads (Thermofisher). Per condition, $5.0*10^5$ cells were seeded in 96-wells plate, which were further diluted to appropriate ratios (1:1 – 1:8). Responder cells (Live, $CD45^+$, $CD3^+$, $CD4^+$, $CD25^-$ and Live, $CD45^+$, $CD3^+$, $CD8^+$) were rested overnight. Next, responder cells were labelled with CellTraceViolet, and co-cultured with T_{regs} in cIMDM supplemented with CD3/CD28 beads (1:5 bead cell ratio) for 96 h (without exogenous IL-2).

NK cell degranulation assay

Single cell suspensions of murine LN and lung samples were plated in a 96-wells plate, and incubated in IMDM containing 8% FCS, 100 IU/ml penicillin, 100 μg/ml streptomycin, 0.5% β-mercapto-ethanol, Golgi-Plug and Golgi-Stop (1:1,000; BD Biosciences) and anti-CD107a (clone LAMP-1, 1:200, Biolegend) for 4 h at 37 °C. For stimulation, cells were additionally supplemented with 50 ng/ml PMA, 1 mM ionomycin.

T_{reg}- KEP serum co-culture assay

$5.0*10^4$ splenic KEP T_{regs} sorted from freshly isolated samples were incubated for 96 h in 96-wells plated coated with 5 μg/mL anti-CD3 in IMDM containing 100 IU/ml penicillin, 100 μg/ml streptomycin, 0.5% β-mercapto-ethanol supplemented with 20% serum obtained from end-stage tumor-bearing KEP mice, or naïve littermates. Next, absolute cell counts were determined by flow cytometry as described above.

IL-33 protein analysis

To quantify IL-33 protein in different tissues of KEP mice and littermates, LegendPlex BioAssay (BioLegend) was used according to manufacturers' instruction. Protein lysates from snap frozen tissue were prepared by pulverizing small tissue fragments (1-$2mm^2$), which were incubated in RIPA buffer (50 mM Tris-HCl, pH 7.4, 150 mM NaCl, 1% NP40, 0.5% DOC, 0.1% SDS, 2 mM EDTA) complemented with protease and phosphatase inhibitors (Roche) for 30 minutes at 4 °C. Protein concentration was quantified using the BCA protein assay kit (Pierce). Samples were diluted to 4 mg/mL protein of which 40uL was used as input for IL-33 LegendPlex Bioassay according to manufacturers' instruction. Protein content (pg/mL) was determined using BioLegend LegendPlex analysis software.

Immunohistochemistry

Immunohistochemical analyses were performed by the Animal Pathology facility at the Netherlands Cancer Institute. Formalin-fixed tissues were processed, sectioned and stained as described (Doornebal et al., 2013). In brief, tissues were fixed for 24 h in 10% neutral buffered formalin, embedded in paraffin, sectioned at 4 μm and stained with haematoxylin and eosin (H&E) for histopathological evaluation. H&E slides were digitally processed using the Aperio ScanScope (Aperio). For immunohistochemical analysis, 5 μm paraffin sections were cut, deparaffinized and stained. To score pulmonary metastasis, lung sections were stained for cytokeratin-8 and metastatic nodules were counted by two independent researchers. To score axillary LN metastasis incidence, draining axillary (proper and accessory) LN of mice that did not develop macroscopic LN metastasis were stained for cytokeratin-8. Presence of cytokeratin-8^+ cells ($\geq$1) within LNs was indicative of micro metastatic disease. Stained tissue slides were digitally processed using the Aperio ScanScope. Brightness and contrast for representative images were adjusted equally among groups.

RNAseq sample preparation: T_{regs}

For transcriptome analysis of T_{regs} from end-stage ($225mm^2$) tumor-bearing KEP mice and WT controls, single cell suspensions were prepared from spleens, mammary LNs, lungs, blood, tumor and naïve WT mammary glands as described above. A minimum of 70.000 T_{regs} (Live, $CD45^+$, $CD3^+$, $CD4^+$, $CD25^{high}$) were sorted in RLT buffer with 1% b-mercapto ethanol. Due to low abundance of T_{regs} in WT mice, tissue of 3 mice was pooled for each WT T_{reg} sample prior to sorting. Library preparation was performed as previously described, (Aslam et al., 2020).

RNAseq sample preparation: NK cells

For transcriptome analysis of NK cells of DT/PBS treated tumor-bearing ($100mm^2$) *Foxp3*$^{GFP\text{-}DTR}$ mice, single cells suspensions were prepared from axillary LNs and lungs, as described above. A minimum of 5000 NK cells (Live, $CD45^+$, $CD3^-$, $NKp46^+$, $DX5^+$) were sorted in RLT buffer with 1% β-mercapto-ethanol. Library preparation was performed as previously described (Picelli et al., 2014), using 2100 Bioanalyzer System for library quality control.

RNAseq of T_{reg} and NK cells

Sorted T_{reg} and NK cells were resuspended in RLT buffer + 1% β -mercapto-ethanol. Total RNA was extracted using RNAeasy mini kit (Qiagen). RNA quality and quantity control was performed using Agilent RNA 6000 Pico Kit and 2100 Bioanalyzer System. RNA samples with an RNA Integrity Number >8 were subjected to library preparation. The strand-specific reads (65bp single-end) were sequenced with the HiSeq 2500 machine. Demultiplexing of the reads was performed with Illumina's bcl2fastq. For T_{reg} RNAseq, demultiplexed reads were aligned against the mouse reference genome (build 38) using TopHat (version 2.1.0, bowtie 1.1). TopHat was supplied with a known set of gene models (Ensembl version 77) and was guided to use the first-strand as the library-type. As

additional parameters –prefilter-multihits and –no coverage were used. For NK cell RNAseq, demultiplexed reads were aligned against the mouse reference genome (build 38) using Hisat2. Hisat2 was supplied with a known set of gene models (Ensembl version 87).

RNAseq analysis

In order to count the number of reads per gene, a custom script, itreecount (https://github.com/NKI-GCF/itreecount), has been used. This script is based on the same concept as HTSeq-count. A list of the total number of uniquely mapped sequencing reads for each gene that is present in the provided Gene Transfer Format (GTF) file was generated. For T_{reg} RNAseq, differential expression was performed using the R package Limma/Voom on normalized counts. Resulting p-values are corrected for multiple testing. A gene was considered differentially expressed if the p-value <0.05, and read counts >30 in all samples of a group.

For PCA the genes that have no expression across all samples within the dataset were removed. Furthermore, the analysis was restricted to only those genes that have at least two counts per million (CPM) value, calculated via edgeR package (3.30.3) using 'cpm' function in all samples from the included conditions and in this way lowly abundant genes were excluded. PCA was performed using the 'prcomp' function on variance stabilizing transformed data with the 'vst' function from the DESeq2 package with default arguments and plotted by using ggplot2 package (3.3.3) in R language (version 4.0.2).

Hierarchical cluster analysis for the samples was performed using 'hclust' function with default arguments. Dendrogram was made by using 'dendro_data' function from ggdendro package (0.1.22). Sample to sample distances obtained using 'dist' function on variance stabilizing transformed data were subjected to hierarchical cluster analysis and dendrogram preparation. Normalized counts from DESeqDataSet from the DESeq2 package were subjected to calculate correlation among the samples by using 'cor' function using spearman method in R language (version 4.0.2).

Differential gene expression analysis of NK cells was performed in R language (version 4.0.2) only on relevant samples using edgeR package (3.30.3) and default arguments with the design set either to PBS or DT-treatment group. Lowly abundant genes (< 2 CPM) from all the samples in a specific contrast were excluded. Furthermore, to avoid any biasness due to the variation among the replicates within a group, the analysis was confined to the genes which have read counts (> 2 CPM) among all the replicates from either of the two groups in a specific contrast. Genes were considered to be differentially expressed when the False discovery rate (FDR) was below 0.1 after the Benjamini–Hochberg multiple testing correction. MA plots were generated after differential expression analysis in R language (version 4.0.2).

IPA and GSEA analysis

Pathway enrichment analysis of KEP/WT T_{regs} RNAseq data was performed using Ingenuity Pathway Analysis software (QIAGEN), analyzing differentially expressed genes with q value <0.05 for KEP/WT T_{regs}. Gene Set Enrichment Analysis (GSEA) (Subramanian et al., 2005) was performed using GSEA software (v. 4.0.3) on RNAseq data (transcripts for which read count >30 included) of KEP/WT T_{reg} of indicated tissues, on gene sets obtained from (Magnuson et al., 2018), and mSigDB Hallmark gene sets (Liberzon et al., 2015). Permutations for each gene set was conducted 1000 times to obtain an empirical null distribution.

Human sentinel LN sampling

Viable cells were collected from SLN from ten female patients diagnosed with clinically node negative BrC scheduled to undergo a SLN procedure between February and July 2014, as previously described (van Pul et al., 2019). None of the patients received neoadjuvant chemo- or hormone therapy prior to the SLN procedure. These ten patients were part of a previously described larger cohort (van Pul et al., 2019), and were selected based on availability of (previously unpublished) NK cell flow cytometry data. Axillary healthy LN were retrieved after written informed consent from prophylactic mastectomy specimens (n = 16) in the Antoni van Leeuwenhoek Hospital between 2012-2014. The collection of these samples was also previously described and approved by the local IRB (van Pul et al., 2019).

Preparation of human LN samples

Viable cells were scraped from the cutting surface of a bisected SLN before routine histopathological examination and after confirmation by the pathologist that the SLN was suitable for cell harvesting (i.e. > 0.5 cm), as described (van Pul et al., 2019; Vuylsteke et al., 2002). SLN cells were subsequently washed twice in IMDM supplemented with 10% FCS, 100 I.E./ml sodium penicillin, 100 μg/ml streptomycin sulfate, 2 mM L-glutamine (P/S/G), and 0.01 mM β-mercapto-ethanol, counted, and used for immune phenotyping. FACS staining for surface and intracellular proteins was performed as described (van Pul et al., 2019) and data were acquired on a FACSCalibur flow cytometer (Becton Dickinson). NK cell and T_{reg} frequencies were determined using FlowJo software (version 10.7). See key resources table for antibodies used.

QUANTIFICATION AND STATISTICAL ANALYSIS

Data analyses were performed using GraphPad Prism (version 8). Data show means ± SEM unless stated otherwise. The statistical tests used are described in figure legends. For comparison of two groups of continuous data, Student's T-test and Mann Whitney's T Test were used as indicated. For comparison of a single variable between multiple groups of normally distributed continuous data, we

used one-way ANOVA, followed by indicated post-hoc analyses. For comparison of ≥ 2 variables between multiple groups, two-way ANOVA was used, with Sidak's post-hoc analysis. Fisher's exact test was used to assess significant differences between categorical variables obtained from lymph node metastasis incidence experiments. All tests were performed two-tailed. p values < 0.05 were considered statistically significant. Sample sizes for mouse intervention experiments were predetermined using G*Power software (version 3.1). *In vivo* interventions and RNAseq experiments were performed once with indicated sample sizes, unless otherwise indicated. *In vitro* experiments were repeated independently as indicated, with at least three biological replicates per condition. Asterisks indicate statistically significant differences compared to WT. * $p < 0.05$, ** $p < 0.01$, *** $p < 0.001$, **** $p < 0.0001$.